An FE^2-method for coupled transient diffusion phenomena in concrete

Filip Nilenius, Fredrik Larsson, Karin Lundgren and Kenneth Runesson

Abstract

A coupled FE^2-framework is formulated and employed for simulation of a transient and coupled moisture-chloride ion diffusion problem in concrete. Simulations are carried out on the macroscale, where the material response is obtained concurrently in the computations by introducing a representative volume element (RVE) in the macroscale quadrature points. The RVE, in turn, contains the mesoscale heterogeneities of concrete in terms of cement paste, aggregates and interfacial transition zone (ITZ). In this fashion, the RVE comes to serves as a constitutive model for the macroscale. A numerical example is given to show how the transient macroscale diffusion is influenced by the composition of the mesoscale constituents. Parametric studies were carried out with respect to the aggregate content within the RVE, both including and excluding the ITZ, and the coupling parameters of moisture and chloride ions.

1 Introduction

In the literature on material modeling, there is an increasing interest in multiscale methods, including homogenization techniques, for better predictions of material responses. The advantage of such modeling approaches is that the effects of subscale heterogeneities are possible to account for while keeping the computational costs at a moderate level, see eg. Yuan and Fish (2008); Zohdi and Wriggers (2005); Nemat-Nasser and Hori (1999).

Concrete, used as building material in various civil engineering applications, possesses strong heterogeneities at multiple length scales, cf. Mehta and Monteiro (2006). Hence, computational multiscale methods makes a suitable tool for such a complex material and the literature in this field is abundant. Li et al. (2011) studied how the effective diffusivity of concrete is affected by the aggregate content using a heterogeneous mesoscale model and FE analyzes and Zeng (2007) did similar studies for transient conditions. Hain and Wriggers (2008, 2007) did analogous studies for effective stiffness of concrete and Garboczi (1998) studied transport properties using an analytical multiscale method.

However, modeling of the transient and *coupled* mass transfer in concrete by means of computational homogenization techniques has not to the authors' knowledge been presented in the literature. This coupled action is of importance for durability reasons since ingress of chloride ions can cause corrosion of the reinforcement which may significantly reduce the structure's load carrying capacity. The chloride ions are coupled to the transport of moisture which makes the transient problem coupled, see e.g. Černý and Rovnaníková (2002). A constitutive model was developed by Ababneh (2002) to capture this coupling effect and Suwito et al. (2006) carried out single-scale, moisture-chloride diffusion simulations using Ababneh's model. In Suwito's work, the mesoscale heterogeneity of concrete was included in the model by scaling the diffusion coefficient with a certain factor.

In this paper, an FE^2-method that includes computational homogenization is developed for transient and coupled conditions. By this method, the macroscale characteristics in terms of relative humidity and chloride concentration are obtained concurrently during the computations. In practise, these characteristics are obtained by solving a subscale FE-problem, on a representative volume element (RVE), introduced in the macroscale quadrature points (typically Gauss-points). Such FE^2-method is required when sub-scale material properties are intrinsically non-linear. In case of linear material properties, it would be sufficient to carry out the homogenization *a priori* and use these results in regular FE analyses. Thus, an FE^2-method is a more general framework as it can handle state dependent material properties which is not possible in a priori homogenization.

The adopted FE^2-framework derives from the variational formulation developed in Larsson et al. (2009) for transient heat conduction. Similar work on FE^2-methods for transient problems can be found in Özdemir et al. (2008).

The paper is organized in the following way: In Section 2, the multiscale variational formulation is established for the coupled diffusion problems at hand. The FE-formulation and, in particular, the macroscale algorithmic tangent operators are given in Section 3 based on the cG(1)dG(0)-method. The model of the mesoscale structure is presented in Section 5, and in Section 6 the specific constitutive models are described. Finally, in Section 7 numerical examples of two-scale simulations are given, followed by conclusions and an outlook for further work in Section 8.

2 Variational formulation

As a fundamental basis, we start with the expressions for mass balance of moisture and chloride ions, respectively, which state that

$$\partial_t \Phi_\phi + \boldsymbol{\nabla} \cdot \boldsymbol{J}_\phi = 0 \quad \text{in } \Omega \times [0, T], \tag{1}$$

$$\partial_t \Phi_c + \boldsymbol{\nabla} \cdot \boldsymbol{J}_c = 0 \quad \text{in } \Omega \times [0, T], \tag{2}$$

where $\Omega \subset \mathbb{R}^3$ is an arbitrary spatial domain of unit thickness bounded by Γ, and where $\boldsymbol{\nabla}$ is the spatial gradient with respect to coordinates $\boldsymbol{x}$ in Ω. The moisture and chloride ion content are denoted $\Phi_\phi(\boldsymbol{x}, t)$ and $\Phi_{\mathrm{c}}(\boldsymbol{x}, t)$, respectively, and $\boldsymbol{J}_\phi(\boldsymbol{x}, t)$ and $\boldsymbol{J}_{\mathrm{c}}(\boldsymbol{x}, t)$ denote the moisture and chloride ion flux, respectively. As there are no sink/source terms on the right hand side of Eqs. (1) and (2), it is assumed that moisture and chloride ions are conserved quantities within Ω. Furthermore, we shall choose constitutive relations on the form

$$\Phi_\phi = \Phi_\phi(\phi), \quad \Phi_{\mathrm{c}} = \Phi_{\mathrm{c}}(c), \tag{3}$$

$$\boldsymbol{J}_\phi = \boldsymbol{J}_\phi(\phi, c; \boldsymbol{g}_\phi, \boldsymbol{g}_c), \quad \boldsymbol{J}_{\mathrm{c}} = \boldsymbol{J}_{\mathrm{c}}(\phi, c; \boldsymbol{g}_\phi, \boldsymbol{g}_c), \tag{4}$$

all of which are described in Section 6. We observe that the two expressions in Eq. (4) are cross-coupled with respect to ϕ and c, which in turn makes Eqs. (1) and (2) cross-coupled. By this choice of constitutive models, it is concluded that the relative pore humidity $\phi = \phi(\boldsymbol{x}, t)$ and chloride concentration $c = c(\boldsymbol{x}, t)$, in grams of chlorides per gram cement paste, are the two primary unknown scalar fields.

Since most of the subsequent derivations are analogous for both Eqs. (1) and (2), they will partially be carried out in a generic fashion using the abbreviating notation $z \stackrel{\text{def}}{=} (\phi, c)$ (for readability, we henceforth use the notation of a scalar field for z, although it explicitly comprises of two scalar functions). As a step in obtaining the variational formulation, we introduce the variational forms

$$a(z; \delta z) \stackrel{\text{def}}{=} -\int_\Omega \boldsymbol{\nabla} \delta z \cdot \boldsymbol{J} \, \mathrm{d}\Omega, \quad l(\delta z) \stackrel{\text{def}}{=} -\int_\Gamma \delta z J_{n,z} \, \mathrm{d}\Gamma, \tag{5}$$

where we introduced $\boldsymbol{J} \stackrel{\text{def}}{=} (\boldsymbol{J}_\phi, \boldsymbol{J}_{\mathrm{c}})$. Additionally, we introduce the scalar product between two scalar-valued fields z and v, as well as between two vector-valued fields $\boldsymbol{z}$ and $\boldsymbol{v}$, in the following manner:

$$(z, v) \stackrel{\text{def}}{=} \int_\Omega z \, v \, \mathrm{d}V, \quad (\boldsymbol{z}, \boldsymbol{v}) \stackrel{\text{def}}{=} \int_\Omega \boldsymbol{z} \cdot \boldsymbol{v} \, \mathrm{d}V. \tag{6}$$

We are now in the position to establish the relevant space/time variational forms

$$A(z; \delta z) \stackrel{\text{def}}{=} \int_0^T (\partial_t \Phi, \delta z) + \int_0^T a(z; \delta z) \, \mathrm{d}t + (\delta z|_{t=0^+}, \Phi|_{t=0^+}), \tag{7}$$

$$L(\delta z) \stackrel{\text{def}}{=} \int_0^T l(\delta z) \, \mathrm{d}t + (\delta z|_{t=0^+}, \Phi_0), \tag{8}$$

where $\Phi \stackrel{\text{def}}{=} (\Phi_\phi, \Phi_{\mathrm{c}}) = \Phi(z)$ and $\Phi_0 \stackrel{\text{def}}{=} (\Phi_{0,\phi}(\boldsymbol{x}, t = 0), \Phi_{0,\mathrm{c}}(\boldsymbol{x}, t = 0))$ corresponding

to initial state. As to the solution space $\mathbb{Z}$ and the corresponding test space $\mathbb{Z}^0$, which contain the subscale fluctuation features, these are defined as $\mathbb{Z} = \{z \in \check{\mathbb{H}}(\Omega \times [0,T]) : z = z_p \text{ on } \Gamma_D\}$ and $\mathbb{Z}^0 = \{z \in \mathbb{Z} : z = 0 \text{ on } \Gamma_D\}$ where $\check{\mathbb{H}}$ denotes the appropriate (Hilbert) space of sufficiently regular functions in the whole space/time domain $\Omega \times [0,T]$.

It is now possible to formulate the variational problem of Eqs. (1) and (2) on the generic (and abstract) form: Find $z \in \mathbb{Z}$ such that

$$A(z;\delta z) = L(\delta z) \quad \forall \delta z \in \mathbb{Z}^0. \tag{9}$$

2.1 Multiscale formulation

The multiscale formulation derived in the following subsections was developed in Larsson et al. (2009) for transient heat flow and is here adopted for diffusion type phenomena. For the multiscale formulation, we introduce a formal splitting of the total solution in an additively manner as $z = z^{\mathrm{M}} + z^{\mathrm{s}}$, corresponding to the macroscale solution z^{M} and subscale solution, z^{s}, which contains the fluctuations of the total solution. It should be noted that z^{M} is much smoother than z^{s}. Furthermore, we assume that $z = z^{\mathrm{M}}$ on Γ, hence $z^{\mathrm{s}} = 0$ on Γ.

It is useful to introduce a formal decoupling between z^{s} and z^{M}, which leads to a model error from the macroscale perspective. The coupling can be formally expressed as the implicit relation $z \approx \tilde{z}^{\mathrm{s}} \stackrel{\text{def}}{=} \tilde{z}^{\mathrm{s}}\{z^{\mathrm{M}}\}$, where $\{(\bullet)\}$ denotes implicit functional dependence on $(\bullet)$. This dependence is in practise achieved by imposing suitable boundary conditions on $\Gamma_\square$ (definition in Section 2.2). We have the representation

$$\tilde{z}\{z^{\mathrm{M}}\} \approx z^{\mathrm{M}} + z^{\mathrm{s}}\{z^{\mathrm{M}}\}, \tag{10}$$

and can now reformulate Eq. (9) by the approximative problem: Find $\tilde{z}\{z^{\mathrm{M}}\} \in \tilde{\mathbb{Z}}$ such that

$$A(\tilde{z}\{z^{\mathrm{M}}\};\delta\tilde{z}\{z^{\mathrm{M}}\}) = L(\delta\tilde{z}\{z^{\mathrm{M}}\}) \quad \forall \delta\tilde{z} \in \tilde{\mathbb{Z}}^0. \tag{11}$$

The variation $\delta\tilde{z}$, see Remark 1, can be expressed as

$$\delta\tilde{z}\{z^{\mathrm{M}}\} = \delta\tilde{z}^{\mathrm{M}} + \delta\tilde{z}^{\mathrm{s}}\{z^{\mathrm{M}}\}, \tag{12}$$

and Eq. (11) can thus be rewritten as

$$A(\tilde{z}\{z^{\mathrm{M}}\};\delta z^{\mathrm{M}}) + A(\tilde{z}\{z^{\mathrm{M}}\};\delta\tilde{z}^{\mathrm{s}}\{z^{\mathrm{M}}\}) = L(\delta z^{\mathrm{M}}) + L(\delta\tilde{z}^{\mathrm{s}}\{z^{\mathrm{M}}\}) \quad \forall \delta z^{\mathrm{M}} \in \mathbb{Z}^{M,0}. \tag{13}$$

Next, we make the important assumption that it is possible to choose prolongation

conditions such that Eq. (13) can be split into two equations corresponding to the macro- and mesoscale, respectively, i.e.

$$A(\tilde{z}\{z^{\mathrm{M}}\};\delta z^{\mathrm{M}}) = L(\delta z^{\mathrm{M}}) \quad \forall \delta z^{\mathrm{M}} \in \mathbb{Z}^{M,0}, \tag{14}$$

$$R(\tilde{z},\delta\tilde{z}^{\mathrm{s}}) \stackrel{\mathrm{def}}{=} L(\delta\tilde{z}^{\mathrm{s}}\{z^{\mathrm{M}}\}) - A(\tilde{z}\{z^{\mathrm{M}}\};\delta\tilde{z}^{\mathrm{s}}\{z^{\mathrm{M}}\}) = 0 \quad \forall \delta z^{\mathrm{M}} \in \mathbb{Z}^{M,0}. \tag{15}$$

Remark 1 *We introduce the variation as the Gateaux-derivative* $\delta\tilde{z}^s\{z^M\} = (\tilde{z}^s)'\{z^M;\delta z^m\} \stackrel{\mathrm{def}}{=} \dfrac{\partial}{\partial\epsilon}\tilde{z}^s\{z^M + \epsilon\delta z^M\}_{|_{\epsilon=0}}$

Remark 2 *The condition in Eq. (15) corresponds to the Hill-Mandel macro-homogeneity condition, which ensures that the virtual-work.* □

Remark 3 *In Section 2.3 it will be shown that the split of Eq. (13) into Eqs. (14) and (15) is valid for the choice of Dirichlet boundary conditions on the RVE.*

2.2 Macroscale problem - First order homogenization

The (generic) variational forms in Eqs. (14) and (15) will be used to develop the full multiscale framework. To achieve this, we need to invoke the concepts of *homogenization* and *representative volume element*, (RVE), which will be presented in the following subsection.

We first assume that the mesoscale features are well represented within an RVE occupying the domain $\Omega_\square \subset \Omega$ bounded by $\Gamma_\square$, and that the center of the RVE is associated with a macroscale coordinate $\bar{\boldsymbol{x}}$. Furthermore, we assume that the macroscale scalar fields ϕ and c vary linearly within the RVE, cf. Figure 1. Hence, we have the representations

$$z^{\mathrm{M}}(\boldsymbol{x};\bar{\boldsymbol{x}}) = \bar{z}(\bar{\boldsymbol{x}}) + \bar{\boldsymbol{g}}(\bar{\boldsymbol{x}})\cdot[\boldsymbol{x}-\bar{\boldsymbol{x}}] \quad \forall \boldsymbol{x} \in \Omega_\square, \tag{16}$$

with the corresponding variation

$$\delta z^{\mathrm{M}}(\boldsymbol{x};\bar{\boldsymbol{x}}) = \delta\bar{z}(\bar{\boldsymbol{x}}) + \delta\bar{\boldsymbol{g}}(\bar{\boldsymbol{x}})\cdot[\boldsymbol{x}-\bar{\boldsymbol{x}}] \quad \forall \boldsymbol{x} \in \Omega_\square, \tag{17}$$

and, consequently, we have the identities

$$\bar{z}(\bar{\boldsymbol{x}},t) = z^{\mathrm{M}}(\bar{\boldsymbol{x}};\bar{\boldsymbol{x}},t), \quad \bar{\boldsymbol{g}}(\bar{\boldsymbol{x}},t) = \boldsymbol{\nabla} z^{\mathrm{M}}(\bar{\boldsymbol{x}},t) \stackrel{\mathrm{def}}{=} \bar{\boldsymbol{\nabla}}\bar{z}(\bar{\boldsymbol{x}},t). \tag{18}$$

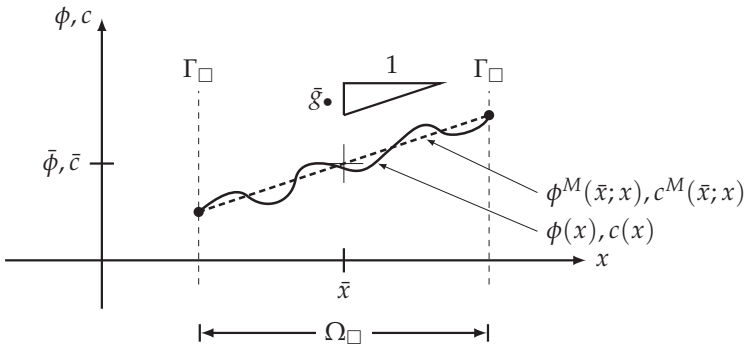

Figure 1: *1D illustration of $z^M = (\phi^M, c^M)$ and their linear variations within $\Omega_\square$.*

Upon inserting the variation δz^{M} in Eq. (17) into Eq. (14), while remembering the definitions in Eqs. (7) and (8), we obtain

$$(\delta z^{\mathrm{M}}, \partial_t \Phi(\tilde{z})) = (\delta \bar{z}, \partial_t \bar{\Phi}) + (\delta \bar{\boldsymbol{g}}, \partial_t \bar{\bar{\boldsymbol{\Phi}}}), \tag{19}$$

$$a(\tilde{z}; \delta z^{\mathrm{M}}) = -(\delta \bar{\boldsymbol{g}}, \bar{\boldsymbol{J}}), \tag{20}$$

$$l(\delta z^{\mathrm{M}}) = -\int_{\Gamma_{\mathrm{N}}} \delta \bar{z} \bar{q}_p \, \mathrm{d}\Gamma. \tag{21}$$

The pertinent homogenized quantities, see Remark 4, are given as the implicit relations in terms of the macroscale variables $\bar{z}$ and $\bar{\boldsymbol{g}}$:

$$\bar{\boldsymbol{J}}\{\bar{z}, \bar{\boldsymbol{g}}\} = \langle \boldsymbol{J} \rangle_\square, \quad \bar{\Phi}\{\bar{z}, \bar{\boldsymbol{g}}\} = \langle \Phi \rangle_\square, \tag{22}$$

$$\bar{\bar{\boldsymbol{\Phi}}}\{\bar{z}, \bar{\boldsymbol{g}}\} \overset{\mathrm{def}}{=} \langle \Phi [\boldsymbol{x} - \bar{\boldsymbol{x}}] \rangle_\square = \langle \Phi \boldsymbol{x} \rangle_\square - \bar{\Phi} \bar{\boldsymbol{x}}, \tag{23}$$

where it is noted that $\bar{\Phi} \overset{\mathrm{def}}{=} (\bar{\Phi}_\phi, \bar{\Phi}_{\mathrm{c}})$ pertains to the scalar-valued storage terms, whereas $\bar{\bar{\boldsymbol{\Phi}}}$ represents the vector-valued quantities $(\bar{\bar{\Phi}}_\phi, \bar{\bar{\Phi}}_{\mathrm{c}})$.

We are now able to establish the macroscale variational forms

$$\bar{A}\{\bar{z},\delta\bar{z}\} \overset{\text{def}}{=} \int_0^T (\delta\bar{z},\partial_t\bar{\Phi})\,\mathrm{d}t - \int_0^T (\bar{\boldsymbol{\nabla}}\delta\bar{z},\bar{\boldsymbol{J}})\,\mathrm{d}t + (\bar{\Phi}|_{t=0^+},\delta\bar{z}|_{t=0^+}) + \int_0^T (\bar{\boldsymbol{\nabla}}\delta\bar{z},\partial_t\bar{\bar{\boldsymbol{\Phi}}})\,\mathrm{d}t + (\bar{\bar{\boldsymbol{\Phi}}}|_{t=0^+},\bar{\boldsymbol{\nabla}}\delta\bar{z}|_{t=0^+}), \tag{24}$$

$$\bar{L}\{\delta\bar{z}\} \overset{\text{def}}{=} \int_0^T \bar{l}(\delta\bar{z})\,\mathrm{d}t + (\bar{\Phi}_0,\delta\bar{z}|_{t=0^+}) + (\bar{\bar{\boldsymbol{\Phi}}}_0,\bar{\boldsymbol{\nabla}}\delta\bar{z}|_{t=0^+}), \tag{25}$$

used to reformulate Eq. (14) into: Find $\bar{z}(\bar{\boldsymbol{x}},t) \in \bar{\mathbb{Z}}$, such that

$$\bar{R}\{\bar{z},\delta\bar{z}\} \overset{\text{def}}{=} \bar{L}\{\delta\bar{z}\} - \bar{A}\{\bar{z},\delta\bar{z}\} = 0 \quad \forall\delta\bar{z} \in \bar{\mathbb{Z}}^0, \tag{26}$$

where $\bar{R}$ denotes the macroscale residual in terms of both moisture content and chloride ion content.

Remark 4 *We introduce the homogenized quantity* $\langle f\rangle_\square$ *of* $f(\boldsymbol{x})$ *as* $\langle f\rangle_\square \overset{\text{def}}{=} \dfrac{1}{|\Omega_\square|}\displaystyle\int_{\Omega_\square} f(\boldsymbol{x})\ \mathrm{d}\Omega_\square, \quad \forall \boldsymbol{x} \in \Omega_\square.$

2.3 Mesoscale problem

2.3.1 Macrohomogeneity condition

Concerning the vanishing residual $R(\tilde{z},\delta\tilde{z}^{\mathrm{s}})$ in Eq. (15), we first note that it can be expressed as an integrated contribution from each RVE (henceforth superscript˜ is dropped for simplification of notation), i.e.

$$R(z,\delta z^{\mathrm{s}}) = \int_\Omega R_\square(z\{z^{\mathrm{M}}\};\delta z^{\mathrm{s}}\{z^{\mathrm{M}}\})(\bar{\boldsymbol{x}})\,\mathrm{d}\Omega, \tag{27}$$

where $R_\square(z;\delta z^{\mathrm{s}})$ is the residual on each RVE. By integrating by parts in the RVE, and using the strong format of the mass balance given in Eqs. (1) and (2), we can show that

$$R_\square(z;\delta z^{\mathrm{s}}) = \frac{1}{|\Omega_\square|}\int_{\Gamma_\square} \delta z^{\mathrm{s}} J_n\,\mathrm{d}\Gamma_\square, \tag{28}$$

where $J_n = \boldsymbol{J}\cdot\boldsymbol{n}$ is the normal outward flux of either moisture or chloride ions. Consequently, to fulfill the Hill-Mandel condition, i.e. for Eq. (15) to hold, it is sufficient that $R_\square(z;\delta z^{\mathrm{s}}) = 0$ on each RVE for each possible $\delta z^{\mathrm{M}} \in \mathbb{Z}^{M,0}$.

2.3.2 Dirichlet boundary conditions on fluctuation field

The most straightforward choice of prolongation condition is defined by homogeneous Dirichlet boundary conditions on the fluctuation field z^{s} on each RVE, i.e. $z^{\mathrm{s}} = 0$ on $\Gamma_\square$.

We may then introduce the pertinent spaces for the subscale (local) solution as follows on any given RVE: $\mathbb{Z}_\square = \mathbb{Z}_\square[\bar{z}, \bar{\boldsymbol{g}}] = \{z \in \check{\mathbb{H}}(\Omega_\square \times [0,T]) : z = \bar{z} + \bar{\boldsymbol{g}} \cdot [\boldsymbol{x} - \bar{\boldsymbol{x}}] \text{ on } \Gamma_\square\}, \mathbb{Z}^0_\square = \mathbb{Z}_\square[\bar{0}, \bar{\boldsymbol{0}}] = \{z \in \mathbb{Z}_\square : z = 0 \text{ on } \Gamma_\square\}$. As to the macrohomogeneity condition, we note that $z^{\mathrm{s}} = 0$ on $\Gamma_\square$. It then follows directly from the boundary integral in Eq. (28) that the residual vanishes and the required constraint is satisfied.

At this point, we can formulate the mesoscale variational problem on the RVE associated with each macroscale position $\bar{\boldsymbol{x}} \in \Omega$. For given z^{M}, find $z \in \mathbb{Z}_\square$ such that

$$R_\square(z, \delta z) \stackrel{\text{def}}{=} L_\square(\delta z) - A_\square(z, \delta z) = 0 \quad \forall \delta z \in \mathbb{Z}^0_\square, \tag{29}$$

where the identities

$$A_\square(z, \delta z) \stackrel{\text{def}}{=} \int_0^T \langle \partial_t \Phi \delta z \rangle_\square + \int_0^T a_\square(z, \delta z)\, \mathrm{d}t + \langle \Phi|_{t=0^+}, \delta z|_{t=0^+} \rangle_\square, \tag{30}$$

$$L_\square(\delta z) \stackrel{\text{def}}{=} \int_0^T l_\square(\delta z)\, \mathrm{d}t + \langle \Phi_0, \delta z|_{t=0^+} \rangle, \tag{31}$$

were introduced.

Remark 5 *It has been shown, by e.g. Zohdi and Wriggers (2005), that Dirichlet type BCs yield an upper bound on the effective diffusivity of the RVE and that Neumann type BCs yield a lower bound.*

3 FE-formulation

3.1 Mesoscale problem

Here, we will use the cG(1)dG(0)-method, cf. Eriksson et al. (1996), corresponding to Euler-backward time-stepping scheme for time-integration of the mesoscale problem. We introduce the finite elements spaces $\mathbb{Z}_{\square,h} \stackrel{\text{def}}{=} {}^n\mathbb{Z}_{\square,h}$ associated with the time interval $I_n = (t_{n-1} - t_n)$ whose length is $\Delta t = t_n - t_{n-1}$. The FE-problem to be solved on the RVE for each time interval I_n now reads: For $n = 1, 2, ..., N$, find ${}^n z \in \mathbb{Z}_{\square,h}$ such that

$$\begin{aligned} R_\square({}^n z; \delta z) &= \Delta t l_\square(\delta z) - \Delta t a_\square({}^n z; \delta z) - \langle [{}^n\Phi - {}^{n-1}\Phi] \delta z \rangle_\square \\ &= 0 \quad \forall \delta z \in \mathbb{Z}^0_{\square,h}, \end{aligned} \tag{32}$$

where ${}^n\Phi \stackrel{\text{def}}{=} \Phi({}^n z)$.

In order to obtain a solution to Eq. (32), a generic algorithm is given which employs Newton's method:

$$
\begin{aligned}
(R_\square)'(\bullet;\delta z,\mathrm{d}z) &= -\langle \delta z \Phi'(\bullet)\,\mathrm{d}z\rangle_\square - \Delta t a'_\square(\bullet;\delta z,\mathrm{d}z) \\
&= -\langle \delta z \Phi'(\bullet)\,\mathrm{d}z\rangle_\square + \Delta t\langle \boldsymbol{\nabla}[\delta z]\cdot \boldsymbol{Y}\,\mathrm{d}z\rangle_\square - \Delta t\langle \boldsymbol{\nabla}[\delta z]\cdot \boldsymbol{D}\cdot\boldsymbol{\nabla}[\mathrm{d}z]\rangle_\square,
\end{aligned}
\tag{33}
$$

where we introduced the tangent forms

$$
\langle \Phi'(\bullet)\,\mathrm{d}z\delta z\rangle_\square = \langle \delta z\Phi'\,\mathrm{d}z\rangle_\square \quad \text{with } \Phi' \overset{\text{def}}{=} \frac{\partial \Phi}{\partial z}, \tag{34}
$$

$$
a'_\square(\bullet;\delta z,\mathrm{d}z) = -\langle \boldsymbol{\nabla}[\delta z]\cdot \boldsymbol{Y}\,\mathrm{d}z\rangle_\square + \langle \boldsymbol{\nabla}[\delta z]\cdot \boldsymbol{D}\cdot\boldsymbol{\nabla}[\mathrm{d}z]\rangle_\square, \tag{35}
$$

with the tangent tensors $\boldsymbol{Y}$ and $\boldsymbol{D}$ defined as

$$
\boldsymbol{Y} \overset{\text{def}}{=} \frac{\partial \boldsymbol{J}}{\partial z}, \quad \boldsymbol{D} \overset{\text{def}}{=} -\frac{\partial \boldsymbol{J}}{\partial(\boldsymbol{\nabla} z)}, \tag{36}
$$

who's explicit expressions can be found in Eqs. (A.1) to (A.3).

The algorithm now reads: For $k = 1, 2, ...$, compute

$$
{}^{n}z^{(k+1)}(\boldsymbol{x}) = {}^{n}z^{(k)} + \mathrm{d}z, \tag{37}
$$

where the iterative updates $\mathrm{d}z \in \mathcal{Z}^0_{\square,h}$ are solved from the tangent equations

$$
-(R_\square)'({}^{n}z^{(k)};\delta z,\mathrm{d}z) = R_\square({}^{n}z^{(k)};\delta z) \quad \forall \delta z \in \mathcal{Z}^0_{\square,h}, \tag{38}
$$

until the residual $R_\square({}^{n}z^{(k)};\delta z)$ is below that of a preset tolerance level. The explicit expressions of Eqs. (32) and (33) are found in Eqs. (A.4) to (A.9).

3.2 Macroscale problem

On the macroscale we apply the same cG(1)dG(0)-method and obtain the problem: For $n = 1, 2, ..., N$, find ${}^{n}\bar{z} \in {}^{n}\bar{\mathcal{Z}}$ that is the solution to

$$
\begin{aligned}
\bar{R}\{{}^{n}\bar{z};\delta\bar{z}\} &= \int_{I_n} \bar{I}(\delta z)\,\mathrm{d}t + \Delta t({}^{n}\bar{\boldsymbol{J}}, \bar{\boldsymbol{\nabla}}[\delta\bar{z}]) \\
&\quad - ([{}^{n}\bar{\Phi} - {}^{n-1}\bar{\Phi}], \delta\bar{z}) - \left(\left[{}^{n}\bar{\bar{\boldsymbol{\Phi}}} - {}^{n-1}\bar{\bar{\boldsymbol{\Phi}}}\right], \bar{\boldsymbol{\nabla}}[\delta\bar{z}]\right) \\
&= 0 \quad \forall \delta\bar{z} \in \bar{\mathcal{Z}}^0,
\end{aligned}
\tag{39}
$$

where ${}^{n}\bar{\boldsymbol{J}} \overset{\text{def}}{=} \bar{\boldsymbol{J}}\{{}^{n}\bar{z}, \bar{\boldsymbol{\nabla}}[{}^{n}\bar{z}]\}$, ${}^{n}\bar{\Phi} \overset{\text{def}}{=} \bar{\Phi}\{{}^{n}\bar{z}, \bar{\boldsymbol{\nabla}}[{}^{n}\bar{z}]\}$, ${}^{n}\bar{\bar{\boldsymbol{\Phi}}} \overset{\text{def}}{=} \bar{\bar{\boldsymbol{\Phi}}}\{{}^{n}\bar{z}, \bar{\boldsymbol{\nabla}}[{}^{n}\bar{z}]\}$.

Again, for the macroscale problem we use Newton's method: For iterations $K = 1, 2, ...$, compute the macroscale spatial fiends

$$ {}^{n}\bar{z}^{(K+1)}(\bar{\boldsymbol{x}}) = {}^{n}\bar{z}^{(K)}(\bar{\boldsymbol{x}}) + \mathrm{d}\bar{z}(\bar{\boldsymbol{x}}), \tag{40} $$

where the iterative updates $\mathrm{d}\bar{z} \in \bar{\mathbb{Z}}^0_{\square}$ are solved from the tangent equations

$$ -(\bar{R})'({}^{n}\bar{z}^{(k)}; \delta\bar{z}, \mathrm{d}\bar{z}) = \bar{R}({}^{n}\bar{z}^{(k)}; \delta\bar{z}) \quad \forall \delta\bar{z} \in \bar{\mathbb{Z}}^0_h, \tag{41} $$

until the residual $\bar{R}({}^{n}\bar{z}^{(k)}; \delta\bar{z})$ is below that of a preset tolerance level. Explicitly, Eq. (41) becomes

$$ -(\bar{R}_\phi)'_\phi({}^{n}\bar{\bullet}^{(k)}; \delta\bar{\phi}, \mathrm{d}\bar{\phi}, 0) - (\bar{R}_\phi)'_{\mathrm{c}}({}^{n}\bar{\bullet}^{(k)}; \delta\bar{\phi}, 0, \mathrm{d}\bar{c}) = \bar{R}_\phi({}^{n}\bar{\bullet}^{(k)}; \delta\bar{\phi}) \quad \forall \delta\bar{\phi} \in \mathbb{H}^0, \tag{42} $$

$$ -(\bar{R}_{\mathrm{c}})'_{\mathrm{c}}({}^{n}\bar{\bullet}^{(k)}; \delta\bar{c}, \mathrm{d}\bar{\phi}, 0) - (\bar{R}_{\mathrm{c}})'_\phi({}^{n}\bar{\bullet}^{(k)}; \delta\bar{c}, 0, \mathrm{d}\bar{c}) = \bar{R}_{\mathrm{c}}({}^{n}\bar{\bullet}^{(k)}; \delta\bar{c}) \quad \forall \delta\bar{c} \in \mathbb{C}^0. \tag{43} $$

Next, we introduce the following algorithmic relations

$$ \begin{aligned} \mathrm{d}\bar{\boldsymbol{J}}_\phi &= \bar{\boldsymbol{Y}}_{\phi\phi}\,\mathrm{d}\bar{\phi} + \bar{\boldsymbol{Y}}_{\phi\mathrm{c}}\,\mathrm{d}\bar{c} - \bar{\boldsymbol{D}}_{\phi\phi} \cdot \mathrm{d}\bar{\boldsymbol{g}}_\phi - \bar{\boldsymbol{D}}_{\phi\mathrm{c}} \cdot \mathrm{d}\bar{\boldsymbol{g}}_{\mathrm{c}}, \\ \mathrm{d}\bar{\Phi}_\phi &= \bar{E}_{\phi\phi}\,\mathrm{d}\bar{\phi} + \bar{E}_{\phi\mathrm{c}}\,\mathrm{d}\bar{c} + \bar{\boldsymbol{B}}_{\phi\phi} \cdot \mathrm{d}\bar{\boldsymbol{g}}_\phi + \bar{\boldsymbol{B}}_{\phi\mathrm{c}} \cdot \mathrm{d}\bar{\boldsymbol{g}}_{\mathrm{c}}, \\ \mathrm{d}\bar{\boldsymbol{\Phi}}_\phi &= \bar{\bar{\boldsymbol{E}}}_{\phi\phi}\,\mathrm{d}\bar{\phi} + \bar{\bar{\boldsymbol{E}}}_{\phi\mathrm{c}}\,\mathrm{d}\bar{c} + \bar{\bar{\boldsymbol{B}}}_{\phi\phi} \cdot \mathrm{d}\bar{\boldsymbol{g}}_\phi + \bar{\bar{\boldsymbol{B}}}_{\phi\mathrm{c}} \cdot \mathrm{d}\bar{\boldsymbol{g}}_{\mathrm{c}}, \end{aligned} \tag{44} $$

$$ \begin{aligned} \mathrm{d}\bar{\boldsymbol{J}}_{\mathrm{c}} &= \bar{\boldsymbol{Y}}_{\mathrm{cc}}\,\mathrm{d}\bar{c} + \bar{\boldsymbol{Y}}_{\mathrm{c}\phi}\,\mathrm{d}\bar{\phi} - \bar{\boldsymbol{D}}_{\mathrm{cc}} \cdot \mathrm{d}\bar{\boldsymbol{g}}_{\mathrm{c}} - \bar{\boldsymbol{D}}_{\phi\mathrm{c}} \cdot \mathrm{d}\bar{\boldsymbol{g}}_\phi, \\ \mathrm{d}\bar{\Phi}_{\mathrm{c}} &= \bar{E}_{\mathrm{cc}}\,\mathrm{d}\bar{c} + \bar{E}_{\mathrm{c}\phi}\,\mathrm{d}\bar{\phi} + \bar{\boldsymbol{B}}_{\mathrm{cc}} \cdot \mathrm{d}\bar{\boldsymbol{g}}_{\mathrm{c}} + \bar{\boldsymbol{B}}_{\phi\mathrm{c}} \cdot \mathrm{d}\bar{\boldsymbol{g}}_\phi, \\ \mathrm{d}\bar{\boldsymbol{\Phi}}_{\mathrm{c}} &= \bar{\bar{\boldsymbol{E}}}_{\mathrm{cc}}\,\mathrm{d}\bar{c} + \bar{\bar{\boldsymbol{E}}}_{\mathrm{c}\phi}\,\mathrm{d}\bar{\phi} + \bar{\bar{\boldsymbol{B}}}_{\mathrm{cc}} \cdot \mathrm{d}\bar{\boldsymbol{g}}_{\mathrm{c}} + \bar{\bar{\boldsymbol{B}}}_{\phi\mathrm{c}} \cdot \mathrm{d}\bar{\boldsymbol{g}}_\phi, \end{aligned} \tag{45} $$

all of which are discussed in the following subsection. These relations are used to compute the tangent form $(\bar{R})'({}^{n}\bar{z}; \delta\bar{z})$, and they are given explicitly in Eqs. (A.10) and (A.11).

3.3 Macroscale algorithmic tangent operators

3.3.1 General

To determine the relations in Eqs. (44) and (45), we need to compute the differential $\mathrm{d}\phi = \mathrm{d}\phi^{\mathrm{M}} + \mathrm{d}\phi^{\mathrm{s}}$ in terms of $\mathrm{d}\bar{\phi}$, $\mathrm{d}\bar{\boldsymbol{g}}_\phi$ and $\mathrm{d}\bar{\boldsymbol{g}}_{\mathrm{c}}$, and the differential $\mathrm{d}c = \mathrm{d}c^{\mathrm{M}} + \mathrm{d}c^{\mathrm{s}}$ in terms of $\mathrm{d}\bar{c}$, $\mathrm{d}\bar{\boldsymbol{g}}_{\mathrm{c}}$ and $\mathrm{d}\bar{\boldsymbol{g}}_\phi$. We have that

$$\mathrm{d}\phi^{\mathrm{M}} = \mathrm{d}\bar{\phi} + \mathrm{d}\bar{\boldsymbol{g}}_{\phi} \cdot [\boldsymbol{x} - \bar{\boldsymbol{x}}] = \mathrm{d}\bar{\phi} + \sum_{i=1}^{NDIM} \hat{\phi}^{M(i)}(\boldsymbol{x}) \bar{g}_{\phi,i}, \tag{46}$$

$$\mathrm{d}c^{\mathrm{M}} = \mathrm{d}\bar{c} + \mathrm{d}\bar{\boldsymbol{g}}_{\mathrm{c}} \cdot [\boldsymbol{x} - \bar{\boldsymbol{x}}] = \mathrm{d}\bar{c} + \sum_{i=1}^{NDIM} \hat{c}^{M(i)}(\boldsymbol{x}) \bar{g}_{c,i}, \tag{47}$$

where $NDIM$ is the number of spatial dimensions. The unit fields, $\hat{\phi}^{M(i)}(\boldsymbol{x})$ and $\hat{c}^{M(i)}(\boldsymbol{x})$, are given as

$$\hat{\phi}^{M(i)}(\boldsymbol{x}) = \hat{c}^{M(i)}(\boldsymbol{x}) = \boldsymbol{e}_i \cdot [\boldsymbol{x} - \bar{\boldsymbol{x}}] = x_i - \bar{x}_i. \tag{48}$$

Next, we introduce the following *ansatz* for $\mathrm{d}\phi^{\mathrm{s}}$ and $\mathrm{d}c^{\mathrm{s}}$:

$$\mathrm{d}\phi^{\mathrm{s}}(\boldsymbol{x}) = \hat{\phi}^{\mathrm{s}}_{\bar{\phi}}(\boldsymbol{x})\, \mathrm{d}\bar{\phi} + \hat{\phi}^{\mathrm{s}}_{\bar{\mathrm{c}}}(\boldsymbol{x})\, \mathrm{d}\bar{c} + \sum_{i=1}^{NDIM} \hat{\phi}^{s(i)}_{\bar{g}_{\phi}}(\boldsymbol{x})\, \mathrm{d}\bar{g}_{\phi,i} + \sum_{i=1}^{NDIM} \hat{\phi}^{s(i)}_{\bar{g}_{\mathrm{c}}}(\boldsymbol{x})\, \mathrm{d}\bar{g}_{c,i}, \tag{49}$$

$$\mathrm{d}c^{\mathrm{s}}(\boldsymbol{x}) = \hat{c}^{\mathrm{s}}_{\bar{\mathrm{c}}}(\boldsymbol{x})\, \mathrm{d}\bar{c} + \hat{c}^{\mathrm{s}}_{\bar{\phi}}(\boldsymbol{x})\, \mathrm{d}\bar{\phi} + \sum_{i=1}^{NDIM} \hat{c}^{s(i)}_{\bar{g}_{\mathrm{c}}}(\boldsymbol{x})\, \mathrm{d}\bar{g}_{c,i} + \sum_{i=1}^{NDIM} \hat{c}^{s(i)}_{\bar{g}_{\phi}}(\boldsymbol{x})\, \mathrm{d}\bar{g}_{\phi,i}, \tag{50}$$

and we obtain the expressions for the total differentials, $\mathrm{d}\phi$ and $\mathrm{d}c$, in terms of $\mathrm{d}\phi^{\mathrm{s}}(\boldsymbol{x})$ and $\mathrm{d}c^{\mathrm{s}}(\boldsymbol{x})$:

$$\begin{aligned} \mathrm{d}\phi(\boldsymbol{x}) &= \left[1 + \hat{\phi}^{\mathrm{s}}_{\bar{\phi}}(\boldsymbol{x})\right] \mathrm{d}\bar{\phi} + \hat{\phi}^{\mathrm{s}}_{\bar{\mathrm{c}}}(\boldsymbol{x})\, \mathrm{d}\bar{c} \\ &\quad + \sum_{i=1}^{NDIM} \left(\left[\hat{\phi}^{M(i)}(\boldsymbol{x}) + \hat{\phi}^{s(i)}_{\bar{g}_{\phi}}(\boldsymbol{x})\right] \mathrm{d}\bar{g}_{\phi,i} + \hat{\phi}^{s(i)}_{\bar{g}_{\mathrm{c}}}(\boldsymbol{x})\, \mathrm{d}\bar{g}_{c,i} \right), \end{aligned} \tag{51}$$

$$\begin{aligned} \mathrm{d}c(\boldsymbol{x}) &= [1 + \hat{c}^{\mathrm{s}}_{\bar{\mathrm{c}}}(\boldsymbol{x})]\, \mathrm{d}\bar{c} + \hat{c}^{\mathrm{s}}_{\bar{\phi}}(\boldsymbol{x})\, \mathrm{d}\bar{\phi} \\ &\quad + \sum_{i=1}^{NDIM} \left(\left[\hat{c}^{M(j)}(\boldsymbol{x}) + \hat{c}^{s(i)}_{\bar{g}_{\mathrm{c}}}(\boldsymbol{x})\right] \mathrm{d}\bar{g}_{c,i} + \hat{c}^{s(i)}_{\bar{g}_{\phi}}(\boldsymbol{x})\, \mathrm{d}\bar{g}_{\phi,i} \right), \end{aligned} \tag{52}$$

and we can now evaluate the linearization of $\bar{\boldsymbol{J}}$, $\bar{\Phi}$ and $\bar{\bar{\boldsymbol{\Phi}}}$ in turn. The details to the evaluations are found in Appendix A.4.

3.3.2 Sensitivity fields within RVE

What remains is to establish the "tangent relations" from which the sensitivity fields $\hat{z}^{\mathrm{s}}_{\bar{z}}(\boldsymbol{x})$ and $\hat{z}^{s(i)}_{\bar{g}}(\boldsymbol{x})$ can be solved for any given time based on the FE-discrete format in space/time. We say that the residual in Eq. (32) must hold for any variation of the macroscale field $z^{\mathrm{M}}(\boldsymbol{x})$ in terms of $\mathrm{d}\bar{z}$ and $\mathrm{d}\bar{\boldsymbol{g}}$. Hence, we have the condition

$$R_\square(z;\delta z) = 0, \quad R_\square(z + \mathrm{d}z;\delta z) = 0 \quad \forall z \in \mathbb{Z}^0_{\square,h}, \tag{53}$$

and upon linearization we obtain the pertinent tangent condition

$$(R_\square)'(\bullet;\delta z,\mathrm{d}z) = 0 \quad \forall z \in \mathbb{Z}^0_{\square,h}, \tag{54}$$

whose explicit expression is that of Eq. (33). Equation (54) may be expanded as follows:

$$(R_\square)'_\phi(\bullet;\delta\phi,\mathrm{d}\phi,0) + (R_\square)'_\phi(\bullet;\delta\phi,0,\mathrm{d}c) = 0 \quad \forall\delta\phi \in {}^0_{\square,h}, \tag{55}$$

$$(R_\square)'_{\mathrm{c}}(\bullet;\delta c,0,\mathrm{d}c) + (R_\square)'_\phi(\bullet;\delta c,\mathrm{d}\phi,0) = 0 \quad \forall\delta c \in {}^0_{\square,h}. \tag{56}$$

Now, inserting the expansion of $\mathrm{d}\phi$ and $\mathrm{d}c$ from Eqs. (51) and (52) into Eqs. (55) and (56) and utilizing that the resulting expression must hold for any differential changes in $\mathrm{d}\bar{\phi}$, $\mathrm{d}\bar{c}$, $\mathrm{d}\bar{g}_\phi$ and $\mathrm{d}\bar{g}_c$, we obtain the four sets of equations, found in Appendix A.5, from which the sensitivity fields are solved.

4 Summary of computational algorithm

In the following the computational implementation of the FE^2-formulation, as derived in the previous Section, is given as pseudocode and schematically, see Figure 2. Algorithm 1 treats the macroscale problem, with the global time stepping and Newton iteration to solve $\bar{R}({}^{n}\bar{z}) \approx 0$ in Eq. (39). In each macroscale Gauss point Algorithm 2, which includes the RVE problem, is called. In standard FE-modeling, Algorithm 2 is entirely replaced by a single continuum constitutive model, eg Fick's law. Herein, continuum constitutive models are instead applied to each of the mesoscale material constituents for the RVE problem in Algorithm 2.

Algorithm 1 Macroscale problem

1: **for** timesteps $n = 1, 2, ..., N$ **do** ▷ Time iteration
2: set initial guess of ${}^{n}\bar{z}(\bar{\boldsymbol{x}})$
3: set $K = 0$
4: **while** $\bar{R}({}^{n}\bar{z}) >$ TOL (predefined tolerance level) **do** ▷ Newton iteration
5: compute ${}^{n}\bar{z}^{(K)}$ and $\bar{\boldsymbol{g}}$ in each Gauss point
6: compute homogenized responses, $\bar{\Phi}$, $\bar{\boldsymbol{J}}$, from **Algorithm 2**
7: solve linearized macroscale problem to obtain ${}^{n}\bar{z}^{(K+1)}$ ▷ Eq. (41)
8: compute macroscale residual, $\bar{R}({}^{n}\bar{z}^{(K+1)})$ ▷ Eq. (39)
9: $K = K + 1$
10: **end while**
11: save ${}^{n}\bar{z}(\bar{\boldsymbol{x}})$
12: **end for**

Algorithm 2 RVE problem: $\bar{z}, \bar{\boldsymbol{g}} \rightarrow \bar{\Phi}, \bar{\boldsymbol{J}}, \frac{\partial \bar{\Phi}}{\partial \bar{z}}, \frac{\partial \bar{\Phi}}{\partial \bar{\boldsymbol{g}}}, \frac{\partial \bar{\boldsymbol{J}}}{\partial \bar{z}}, \frac{\partial \bar{\boldsymbol{J}}}{\partial \bar{\boldsymbol{g}}}$.

1: compute Dirichlet BC based on ${}^{n}\bar{z}$ and $\bar{\boldsymbol{g}}$ ▷ Eq. (16)
2: set initial guess of ${}^{n}z(\boldsymbol{x})$
3: set $k = 0$
4: **while** $R_{\square}({}^{n}z) >$ TOL$_{\square}$ **do** ▷ Newton iteration
5: solve linearized RVE problem to obtain ${}^{n}z^{(k+1)}$ ▷ Eq. (38)
6: compute mesoscale residual, $R_{\square}({}^{n}z^{(k+1)})$ ▷ Eq. (32)
7: $k = k + 1$
8: **end while**
9: save ${}^{n}z(\boldsymbol{x})$
10: homogenize RVE response to obtain $\bar{\Phi}$ and $\bar{\boldsymbol{J}}$ ▷ Eqs. (22) and (23)
11: solve sensitivity problem ▷ Eqs. (A.40) to (A.47)
12: determine algorithmic tangent operators, $\frac{\partial \bar{\Phi}}{\partial \bar{z}}, \frac{\partial \bar{\Phi}}{\partial \bar{\boldsymbol{g}}}, \frac{\partial \bar{\boldsymbol{J}}}{\partial \bar{z}}, \frac{\partial \bar{\boldsymbol{J}}}{\partial \bar{\boldsymbol{g}}}$ ▷ Appendix A.4
13: **return** results from lines 10 and 12

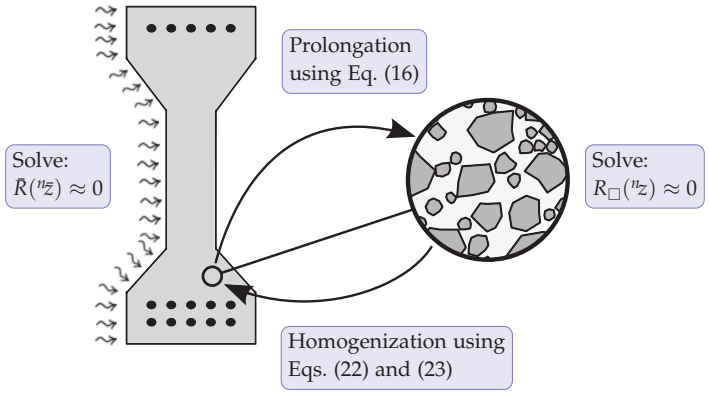

Figure 2: Pictorial representation of the FE^2-algorithm using a concrete beam's cross section (left) with its heterogeneous mesoscale structure (right). This procedure makes the RVE problem a constitutive model for the macroscale domain.

5 Characterization of the mesoscale structure

On the mesoscale, concrete is considered a three-phase composite material, consisting of the cement paste, aggregates and Interfacial Transition Zone (ITZ). Each phase is assumed to be homogenous. The ITZ is introduced as a highly diffusive interface "material" along the perifery of each aggregate particle.

At the core of homogenization analysis is the generation of an SVE (= Statistical Volume Element) of the mesoscale structure of concrete. An SVE is a realization of a stochastic field and is generated from a given statistical representation of the subscale features; however, its size can be considerably smaller than the RVE (= Representative Volume Element) which must be sufficiently large so that any realization gives essentially the same response. For a discussion of the requirements on the RVE and SVE's, see Zohdi and Wriggers (2005). Various strategies for the generation of SVE's have been devised in the literature. Stankowski (1990) used Voronoi polygonization to numerically generate a 2D-structure. This idea was extended to 3D mesostructure by Caballero et al. (2006) in the context of fracture analysis of concrete. CT-scanning technique was used by Hain and Wriggers (2008) to generate 3D microstructures of cement paste.

The strategy used for the numerical generation of 2D structures of SVE's with subsequent FE-meshing is described in detail in Nilenius et al. (2012). The main control parameters of the algorithm are the area fraction of aggregates, denoted n_b, and the sieve curve of aggregates. At the outset, each aggregate particle is an octagon with the radius r. The randomness in shape of the aggregates is generated by adding a random variation to the radius of each corner point in the octagon. Examples of SVE-realizations are shown in Figure 3.

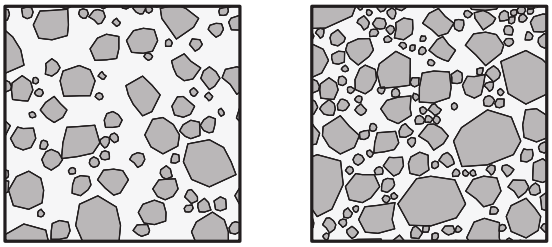

(a) $n_b \approx 50\%$. (b) $n_b \approx 60\%$.

Figure 3: Example SVE realizations.

6 Constitutive relations for the mesoscale materials

6.1 Preliminaries

the transport processes of moisture and chloride ions will be modeled as that of diffusion processes, whereby concentration gradients of moisture and chloride ions are the driving forces on the fine scale. In principle, such transport takes place in all constituents; however, for practical purposes it can be assumed that the aggregates are completely impervious.

The model framework described in Sections 2 and 3 is general in its formulation material-wise, i.e. the constitutive relations needed for $\Phi_\phi(\phi)$, $\Phi_c(c)$, $\boldsymbol{J}_\phi(\phi, c, \boldsymbol{g}_\phi, \boldsymbol{g}_c)$ and $\boldsymbol{J}_c(\phi, c, \boldsymbol{g}_\phi, \boldsymbol{g}_c)$ could be of any type. The benefit is, naturally, that the model could still be employed as new, and more refined, constitutive models are developed. For instance, Černý (2004) argues that the moisture-chloride coupling phenomenon in cement is still an open topic in terms of constitutive modeling and physical understanding. Still, both him and Ababneh (2002) conclude from their experiments that there truly is a cross-coupling between the two quantities. In this work we only consider the case of coupled flux-terms, $\boldsymbol{J}_\phi$ and $\boldsymbol{J}_c$; however, Koniorczyk and Wojciechowski (2009) suggest that the moisture capacity also depends on the chloride concentration, i.e. $\Phi_\phi = \Phi_\phi(\phi, c)$.

In the following subsections, the constitutive models taken from the literature and used for numerical simulations, are described. We conclude from the choice of constitutive models that $\Phi'_{\phi c} = \Phi'_{c\phi} = 0$. It is apparent in Figures 4a, 4b, 6a and 6b that the constitutive models chosen are highly non-linear with respect to their arguments, and for practical reasons of implementation, they have been replaced with multi-linear approximations. One benefit of a multi-linear model is that its derivative is simply a constant.

6.1.1 Diffusion properties of the cement paste

Experimental results by Ababneh et al. (2003) indicate that the transport of moisture and chloride ions are cross-coupled in the *pure cement matrix*. Based on these results, a "quasi-linear" constitutive model was proposed by them as follows:

$$\boldsymbol{J}_\phi(\phi, c; \boldsymbol{g}_\phi, \boldsymbol{g}_c) = -D_\phi(\phi)\boldsymbol{g}_\phi - \varepsilon_{\mathrm{c}} D_{\mathrm{c}}(\phi, c)\boldsymbol{g}_c, \tag{57}$$

$$\boldsymbol{J}_{\mathrm{c}}(\phi, c; \boldsymbol{g}_\phi, \boldsymbol{g}_c) = -\varepsilon_\phi D_\phi(\phi)\boldsymbol{g}_\phi - D_{\mathrm{c}}(\phi, c)\boldsymbol{g}_c, \tag{58}$$

where it is assumed from the outset that the intrinsic diffusion properties (for the pure cement paste), represented by the diffusion coefficients $D_\phi > 0$ and $D_{\mathrm{c}} > 0$, are isotropic. Furthermore, ε_ϕ and ε_{c} are coupling parameters, which are taken as constants according to Suwito et al. (2006) ($\varepsilon_\phi = 0.028$ and $\varepsilon_{\mathrm{c}} = 0.2$), see Remark 6. The expressions Eqs. (57) and (58) can be seen as modifications of Fick's classical law of diffusion.

The pertinent expressions for the state-dependent diffusion coefficients adopted here were proposed, together with values of the parameters α_h, β_h, γ_h, f_1, f_2, f_3, f_4, and f_5, by Xi et al. (1994) and Xi and Bažant (1999). They are as follows:

$$D_\phi(\phi) = \alpha_h + \beta_h \left[1 - 2^{-10^{\gamma_h}[\phi - 1]}\right] \qquad [\mathrm{cm}^2/\mathrm{day}], \tag{59}$$

$$D_{\mathrm{c}}(\phi, c) = f_1(t_0) f_2(g_i) f_3(\phi) f_4(T) f_5(c) \qquad [\mathrm{cm}^2/\mathrm{day}]. \tag{60}$$

How D_ϕ and D_{c} depend on their respective arguments is illustrated in Figures 4a and 4b.

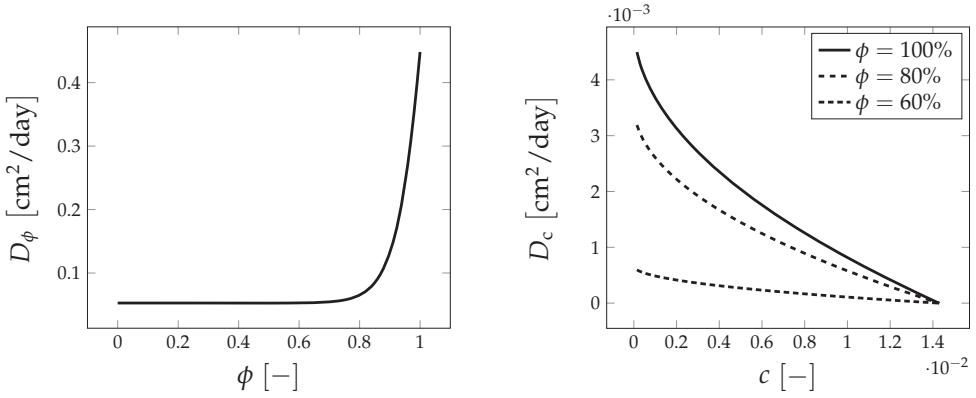

Figure 4: *Functional dependencies of* $\mathbf{D}_{\mathfrak{E}}(\mathfrak{E})$ *and* $\mathbf{D}_c(\mathfrak{E})$ *on* ϕ *and* c*, respectively.*

Remark 6 *We shall require the "compound diffusivity" to be positive definite in the sense that* $\boldsymbol{J}_\phi \cdot \boldsymbol{g}_\phi + \boldsymbol{J}_c \cdot \boldsymbol{g}_c < 0$ *for any* $\boldsymbol{g}_\phi \neq \boldsymbol{0}$ *and* $\boldsymbol{g}_c \neq \boldsymbol{0}$*. This is equivalent to the requirement* $1 - \varepsilon_\phi \varepsilon_c > 0$*, which is, obviously, satisfied for the chosen values of* ε_ϕ *and* ε_c*.*

6.1.2 Diffusion properties of the ITZ

For the ITZ, we assume a constitutive relation with the same structure as that of the cement paste, described in the previous subsection. However, the diffusion coefficients for ITZ do not represent a homogeneous material but rather the net effect of pores and microcracks within a thin zone of thickness h. We treat ITZ as a 1D continuum material in the mesoscale domain, implying that mass transport is allowed only in the plane of the aggregate/cement interface, which is denoted by $\|$, see Figure 5. Consequently, the constitutive relations take the form

$$\boldsymbol{J}_\phi(\boldsymbol{g}_\phi, \boldsymbol{g}_c) = \boldsymbol{J}_{\phi,\|} = -D_{\phi,\mathrm{ITZ}} \boldsymbol{g}_{\|\phi} - \varepsilon_\mathrm{c} D_{\mathrm{c,ITZ}} \boldsymbol{g}_{\|c}, \tag{61}$$

$$\boldsymbol{J}_\mathrm{c}(\boldsymbol{g}_\phi, \boldsymbol{g}_c) = \boldsymbol{J}_{\mathrm{c},\|} = -\varepsilon_\phi D_{\phi,\mathrm{ITZ}} \boldsymbol{g}_{\|\phi} - D_{\mathrm{c,ITZ}} \boldsymbol{g}_{\|c}, \tag{62}$$

where $\boldsymbol{g}_{\|\bullet} = \boldsymbol{g}_\bullet \cdot [\boldsymbol{I} - \boldsymbol{e}_\perp \otimes \boldsymbol{e}_\perp]$. Here, we introduced $\boldsymbol{J}_{\phi,\|}$ and $\boldsymbol{J}_{\mathrm{c},\|}$ as the mass flux vectors along the ITZ; hence, the orthogonal components are zero by construction.

FE-discretization of the ITZ gives the following typical interface element relation

$$\begin{bmatrix} \underline{\boldsymbol{J}}^e_\phi \\ \underline{\boldsymbol{J}}^e_\mathrm{c} \end{bmatrix} = - \begin{bmatrix} \underline{\boldsymbol{K}}^e_{\phi\phi} & \underline{\boldsymbol{K}}^e_{\phi\mathrm{c}} \\ \underline{\boldsymbol{K}}^e_{\mathrm{c}\phi} & \underline{\boldsymbol{K}}^e_{\mathrm{cc}} \end{bmatrix} \begin{bmatrix} \underline{\boldsymbol{\phi}}^e \\ \underline{\boldsymbol{c}}^e \end{bmatrix}, \tag{63}$$

where $\underline{\boldsymbol{\phi}}^e$ and $\underline{\boldsymbol{c}}^e$ are the nodal values of ϕ and c, respectively. Using piecewise linear interpoation of ϕ and c, the submatrices, representing diffusion resistance, take the simple explicit forms

$$\underline{\boldsymbol{K}}^e_{\phi\phi} = \frac{D_{\phi,\mathrm{ITZ}} A_\mathrm{ITZ}}{L_e} \begin{bmatrix} 1 & -1 \\ -1 & 1 \end{bmatrix}, \tag{64}$$

$$\underline{\boldsymbol{K}}^e_{\phi\mathrm{c}} = \varepsilon_\mathrm{c} \frac{D_{\mathrm{c,ITZ}} A_\mathrm{ITZ}}{L_e} \begin{bmatrix} 1 & -1 \\ -1 & 1 \end{bmatrix}, \tag{65}$$

$$\underline{\boldsymbol{K}}^e_{\mathrm{c}\phi} = \varepsilon_\phi \frac{D_{\phi,\mathrm{ITZ}} A_\mathrm{ITZ}}{L_e} \begin{bmatrix} 1 & -1 \\ -1 & 1 \end{bmatrix}, \tag{66}$$

$$\underline{\boldsymbol{K}}^e_{\mathrm{cc}} = \frac{D_{\mathrm{c,ITZ}} A_\mathrm{ITZ}}{L_e} \begin{bmatrix} 1 & -1 \\ -1 & 1 \end{bmatrix}, \tag{67}$$

where A_ITZ is the cross-sectional area of the ITZ layer with unit thickness, and L_e is the length of the ITZ element. The ITZ was assigned a width, h, of 60 [μm] in the FE-model (Rossignolo (2007)), which yields $A_\mathrm{ITZ} = 1 \times 60$ [$\mu\mathrm{m}^2$].

Remark 7 *It is noted that the FE-discretized fields ϕ and c are continuous across the interface elements.* □

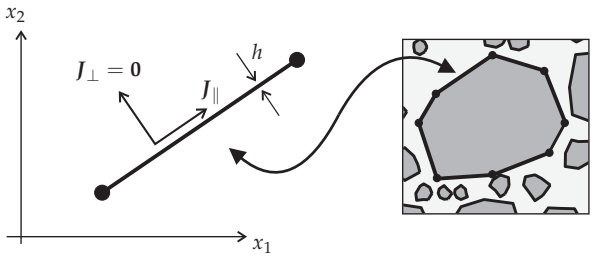

Figure 5: *ITZ interface elements along the perifery of each aggregate.*

6.2 Moisture and chloride capacities for the mesoscale materials

The constitutive model for $\Phi_\phi(\phi)$ is taken from Bažant and Najjar (1972) which states that

$$\Phi_\phi(\phi) = \frac{C_m k V_m H}{(1 - kH)(1 + (C_m - 1)kH)}, \tag{68}$$

where $\phi = v/v_s(T)$ is the relative humidity and C_m, k and V_m are material parameters. v is the vapor content in the cement pores and v_s is the vapor content at saturation as a function of temperature T.

The constitutive model for $\Phi_c(c)$ is taken from Tang and Nilsson (1993) which relates the bound chloride ions, C_b, to the free ones, c, in the following manner:

$$C_b(c) = 10^\alpha c^\beta, \tag{69}$$

which yields

$$\Phi_c(c) \stackrel{\text{def}}{=} c + C_b(c) = c + 10^\alpha c^\beta, \tag{70}$$

where α and β material parameters. In Figures 6a and 6b, the constitutive descriptions for $\Phi_\phi(\phi)$ and $\Phi_c(c)$ are plotted, respectively.

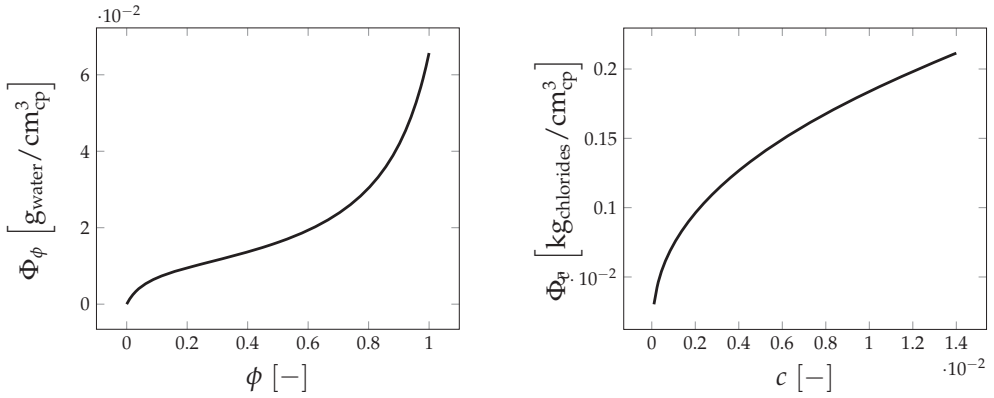

Figure 6: *Constitutive models for Φ_ϕ and Φ_c. Subindex "*cp*" is for cement paste.*

Moisture and chloride capacities for aggregates and ITZ are assumed to be zero in the model, i.e. $\Phi_\phi = \Phi_{\mathrm{c}} = 0$.

7 Numerical example

7.1 Preliminaries

As a numerical example we consider a discretizised macroscale domain as depicted in Figure 7. On the left vertical boundary, convection boundary conditions are applied whereas all other boundaries are insulated. The convective boundary conditions are of the type

$$\bar{J}_{\phi,n} = -\alpha_{\bar{\phi}}(\bar{\phi} - \bar{\phi}_\infty), \tag{71}$$

$$\bar{J}_{\mathrm{c},n} = -\alpha_{\bar{c}}(\bar{c} - \bar{c}_\infty), \tag{72}$$

where $\alpha_{\bar{\phi}}$ and $\alpha_{\bar{c}}$ are convection coefficients of moisture and chloride ions, respectively.

We shall be interested in studying the time evolutions of the macroscale fields of $\bar{\phi}$ and $\bar{c}$ for different mesoscale setups within the RVE. In particular, we want to establish $\bar{\phi}$'s and $\bar{c}$'s dependencies on the aggregate content, n_b, within the RVE, and the effect of including/excluding the ITZ. Furthermore, a study of the coupling parameters, ε_ϕ and ε_{c} will be carried out.

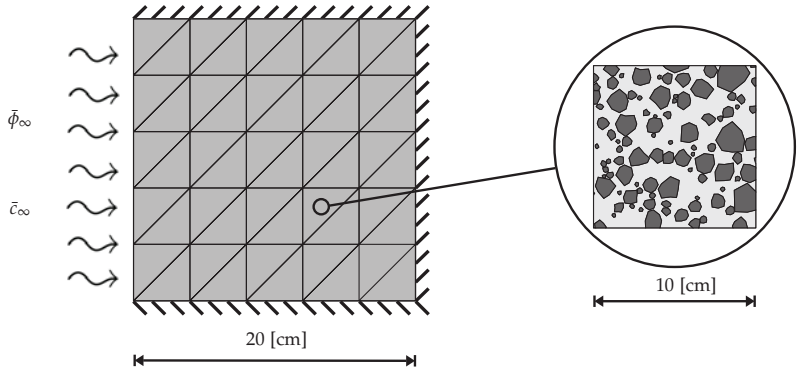

Figure 7: *Discretizised macroscale domain (left) with its embedded heterogenous mesoscale structure (right).*

In Table 1, input parameters used for the numerical simulation are given.

Table 1: Input parameters

Parameter	Description	Value	Unit
$\bar{\phi}_\infty$	ambient humidity	80	%
$\bar{c}_\infty$	ambient chloride concentration	1	%
$\bar{\phi}_{\text{in}}$	initial humidity	60	%
$\bar{c}_{\text{in}}$	initial chloride concentration	0.004	%
$\alpha_{\bar{\phi}}$	humidity convection coefficient	0.05	$\text{cm}^{-2}\,\text{s}^{-1}$
$\alpha_{\bar{c}}$	chloride cons. convection coefficient	0.025	$\text{cm}^{-2}\,\text{s}^{-1}$
ε_ϕ	coupling parameter	0.028	-
ε_{c}	coupling parameter	0.2	-

7.2 Choice of RVE

The choice of RVE used for the numerical simulations is a delicate one since it will influence the time evolution of $\bar{\phi}$ and $\bar{c}$. In fact, $\bar{\phi}$ and $\bar{c}$ are implicit functions of the RVE. For a chosen sieve curve adapted for 2D as given in Figure 8 Nilenius et al. (2012) concluded that an RVE of minimum $10 \times 10\,\text{cm}^2$ is required, based on convergence study. This RVE-size was used in this numerical example. Furthermore, the RVEs generated by the algorithm are random in topology meaning that only using one RVE is not sufficient since it is not actually *representative*, by construction. To really have a representative volume element, it would be necessary to invoke a number of RVE

realizations for each Gauss-point and to extract the mean response of all those RVEs. However, to reduce the computational effort this procedure requires, the RVE with the response closest to the mean response, of a set of RVE realizations, was consistently used for the numerical examples.

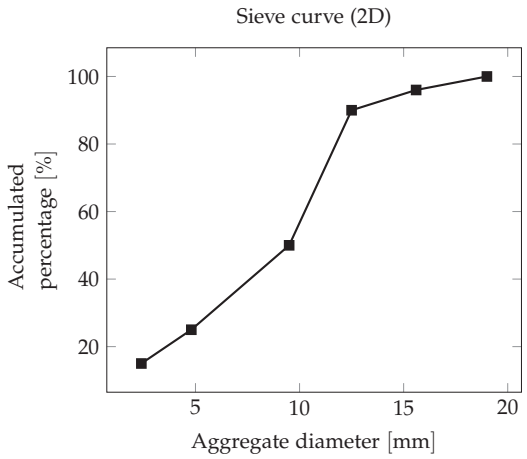

Figure 8: Apparent sieve curves for the model.

7.3 Computational results

In Figure 9, snapshots of the transient solution of $\bar{\phi}$ are given for a certain time-step. As expected, for the given macroscopic boundary conditions, the mass flux is purely one dimensional. However, on the mesoscale diffusion is a 2D problem, as can be seen in the bottom right RVE.

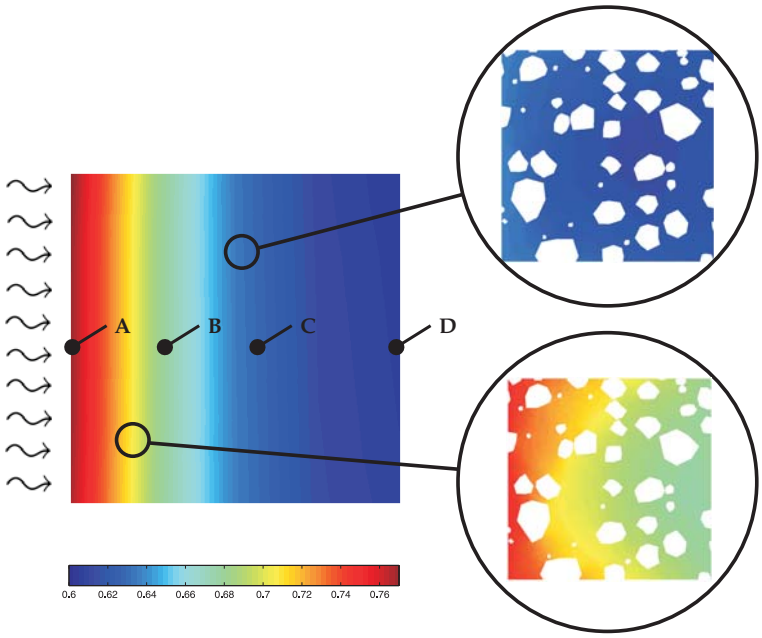

Figure 9: *Snapshot of transient solution to macroscale relative humidity, $\bar{\phi}$, for a given time step. The smooth solution on the macroscale (left) is obtained by homogenization of the non-smooth RVE responses (right).*

In Figures 10 and 11, the time evolution of $\bar{\phi}$ and $\bar{c}$ are presented for varying n_b. Figures 10 and 11 show that the diffusion rate is decreased at the back-end of the macroscale domain for increasing n_b, cf. point D in Figure 10. Furthermore, the effect of aggregates appears to be greater for the chloride ion problem by comparing Figures 10 and 11. This behavior is due to difference in the Φ_ϕ / D_ϕ and Φ_c / D_c ratios.

It was concluded in Nilenius et al. (2012) that the macroscopic diffusivity is decreased for increasing n_b, in the case of stationary conditions. Hence, one would perhaps expect the increase in $\bar{\phi}$ at the front-end to be lower for concrete than for pure cement paste. However, concrete has lower storage capacity than pure cement; thus, saturation is reached faster at the front-end. Consequently, the influx will quickly be reduced at the front-end for concrete due to the formulation of the boundary condition in Eq. (71). When the ITZ is included, this behavior is further pronounced.

The consequence of this behavior is that a saturated ”barrier” of both moisture and chlorides is created near the convective boundary when aggregates are present in the RVE. For the back-end of the macroscale domain, this results in a slow time evolution of $\bar{\phi}$ and $\bar{c}$.

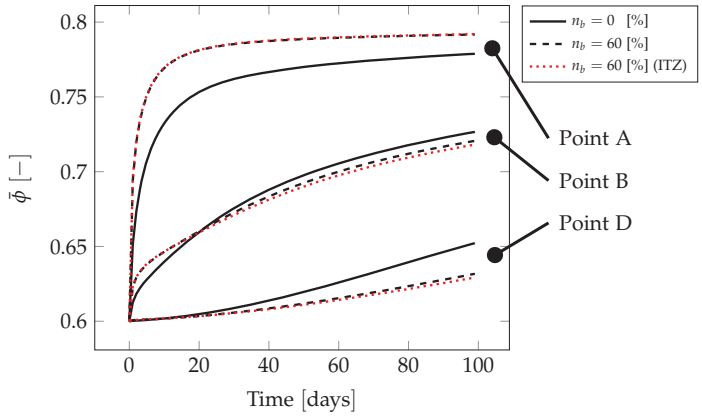

Figure 10: *Time evolution of macroscale relative humidity,$\bar{\phi}$, for varying values of n_b, in different points in the macroscale domain. The red line has the ITZ included in the RVE. Point A,B and D are defined in Figure 9.*

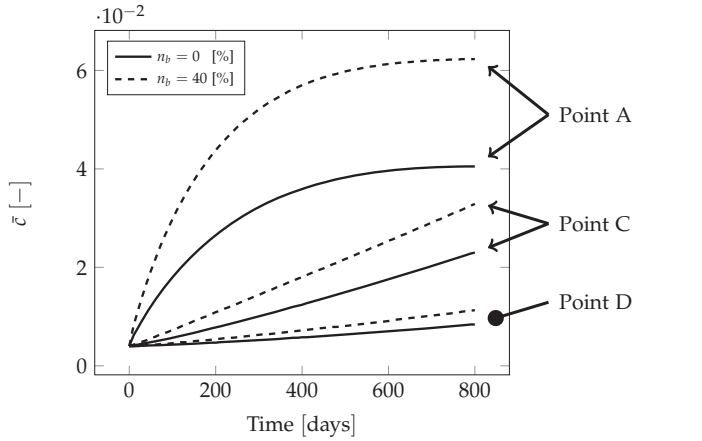

Figure 11: *Time evolution of macroscale chloride concentration, $\bar{c}$, for varying values of n_b, in different points in the macroscale domain. Point A,C and D are defined in Figure 9.*

In Figure 12, the time evolution of $\bar{c}$ is shown, for the coupled and uncoupled cases. For the corresponding time evolution of $\bar{\phi}$ in Figure 13, no significant difference between the coupled/uncoupled cases could be observed. The reason for this behavior is that the term $\varepsilon_c D_c(\phi, c)\boldsymbol{g}_c$ in Eq. (57), gives a small contribution to $\boldsymbol{J}_\phi$ mainly due to differens in magnitude between D_ϕ and D_c. This indicates that the numerical values of ε_ϕ and ε_c need further verification when included in this model, to really capture the coupling

effect which has been apparent in experiments.

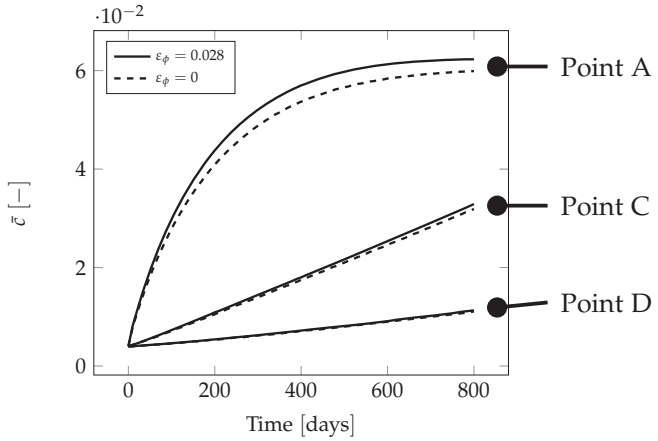

Figure 12: *Time evolution of macroscale chloride concentration, $\bar{c}$, for varying values of ε_ϕ, in different points in the macroscale domain for $n_b = 40$ [%]. Point A,B and D are defined in Figure 9.*

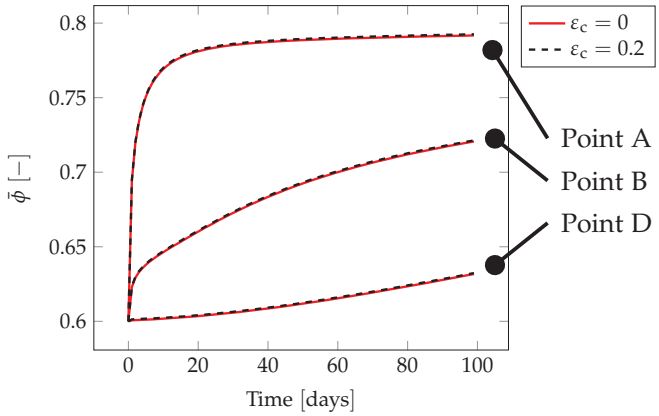

Figure 13: *Time evolution of macroscale relative humidity, $\bar{\phi}$, for varying values of ε_c, in different points in the macroscale domain for $n_b = 40$ [%]. Point A,B and D are defined in Figure 9.*

7.4 FE^2 - FE^1 comparison

To validate the FE^2-computational scheme, we compare the numerical FE^2 results by the corresponding ones obtained by conventional FE-analysis (here denoted FE^1); i.e. when the material constitutive relations are applied directly at the macroscale Gauss-points and no subscale RVE-problem is introduced what-so-ever. For this example we consider the case of pure cement paste, i.e. for $n_b \stackrel{\text{def}}{=} 0$, implying that the RVE used in the FE^2-scheme is truly homogeneous. The reason for choosing $n_b = 0$ is to see how the RVE-problem, as an constitutive model, affects the resolution of the macroscale solution. If $n_b > 0$ was chosen we would additionally have had to make an assumption on the effective diffusivity of the FE^1 model which, in turn, could imply that any difference between the FE^2 and FE^1 models would steam merely from the choice of n_b and how the *a priori* homogenization of the FE^1 model was carried out. Moreover, using a priori homogenization would only be valid for linear material properties. In Figure 14, a comparison between the different numerical schemes is shown.

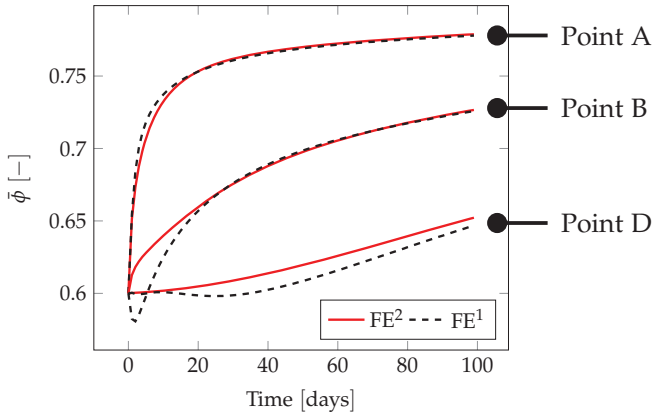

Figure 14: *Time evolution of macroscale relative humidity, $\bar{\phi}$, for the different schemes, FE^2 and FE^1 (conventional FE-modeling) where $n_b = 0\,\%$ for both models. Point A,B and D are defined in Figure 9.*

It can be observed in Figure 14 that $\bar{\phi}$ decreases below the initial value early in the simulation for the FE^1-model (numerical artifact), cf. points B and D, which is not reasonable from a physical standpoint since $\bar{\phi}_\infty = 80\,\%$. This phenomena is not observed in the FE^2 model which implies a better resolution of $\bar{\phi}(t)$. As time progress, the FE^1-model stabilizes and both models converge towards the same solution.

8 Conclusions and Outlook

Implementation of an FE^2-model for numerical simulations of coupled moisture and chloride ion diffusion in concrete was carried out in this work. The model suggests how the smooth macroscale fields $\bar{\phi}$ and $\bar{c}$ can be solved for during transient conditions while accounting for the mesoscale heterogeneities of the material. In practice, this is achieved by introducing a representative volume element (RVE) of concrete as a constitutive model in the Gauss-points on the macroscale. The RVE contains the mesoscale constituents in terms of cement paste, aggregate and interfacial transition zone (ITZ).

The results in Figures 10 and 11 show that the influence of aggregates, and ITZ, on $\bar{\phi}$ and $\bar{c}$ is complex during transient conditions. The presence of aggregates can both decrease and increase the diffusion rate, depending on the location in the macroscale domain. Additionally, the influence of gravel is different in magnitude for the different quantities $\bar{\phi}$ and $\bar{c}$, cf Point D for $n_b = 0\,\%$ and $n_b = 60\,\%$ in Figures 10 and 11. Consequently, the importance of having an accurately modelled mesoscale setup within the RVE, both in terms of aggregate representation and ITZ, is evident.

It is further observed from the numerical simulations that the coupling effect between $\bar{\phi}$ and $\bar{c}$ is small, cf. Figures 12 and 13. This fact stems from the formulation of the coupling formulation and chosen parameter values in the constitutive relations, Eqs. (57) and (58), as discussed in Section 7.3. The FE^2-method proposed herein still needs validation with experimental data in order to be utilized as a tool for predicting moisture/chloride diffusion in a realistic manner.

A

A.1 Mesoscale tangent tensors

The explicit expressions for $\boldsymbol{Y}$, $\boldsymbol{D}$ and Φ' are

$$\boldsymbol{Y}_{\phi\phi} \stackrel{\text{def}}{=} \frac{\partial \boldsymbol{J}_\phi}{\partial \phi}, \quad \boldsymbol{Y}_{\phi \mathrm{c}} \stackrel{\text{def}}{=} \frac{\partial \boldsymbol{J}_\phi}{\partial c}, \quad \boldsymbol{Y}_{\mathrm{c}\phi} \stackrel{\text{def}}{=} \frac{\partial \boldsymbol{J}_\mathrm{c}}{\partial \phi}, \quad \boldsymbol{Y}_{\mathrm{cc}} \stackrel{\text{def}}{=} \frac{\partial \boldsymbol{J}_\mathrm{c}}{\partial c} \tag{A.1}$$

$$\boldsymbol{D}_{\phi\phi} \stackrel{\text{def}}{=} -\frac{\partial \boldsymbol{J}_\phi}{\partial (\boldsymbol{g}_\phi)}, \quad \boldsymbol{D}_{\phi \mathrm{c}} \stackrel{\text{def}}{=} -\frac{\partial \boldsymbol{J}_\phi}{\partial (\boldsymbol{g}_c)}, \quad \boldsymbol{D}_{\mathrm{c}\phi} \stackrel{\text{def}}{=} -\frac{\partial \boldsymbol{J}_\mathrm{c}}{\partial (\boldsymbol{g}_\phi)}, \quad \boldsymbol{D}_{\mathrm{cc}} \stackrel{\text{def}}{=} -\frac{\partial \boldsymbol{J}_\mathrm{c}}{\partial (\boldsymbol{g}_c)}, \tag{A.2}$$

$$\Phi'_{\phi\phi} \stackrel{\text{def}}{=} \frac{\partial \Phi_\phi}{\partial \phi}, \quad \Phi'_{\phi \mathrm{c}} \stackrel{\text{def}}{=} \frac{\partial \Phi_\phi}{\partial c}, \quad \Phi'_{\mathrm{c}\phi} \stackrel{\text{def}}{=} \frac{\partial \Phi_\mathrm{c}}{\partial \phi}, \quad \Phi'_{\mathrm{cc}} \stackrel{\text{def}}{=} \frac{\partial \Phi_\mathrm{c}}{\partial c}. \tag{A.3}$$

A.2 Mesoscale (tangent) residuals

The explicit expressions of Eqs. (32) and (33) become

$$\begin{aligned} R_{\phi,\square}(\phi, c; \delta\phi) = {} & \Delta t l_\square(\delta\phi) - \Delta t \langle \boldsymbol{\nabla}[\delta\phi] \cdot \boldsymbol{J}_\phi \rangle_\square \\ & - \langle \delta\phi [\Phi_\phi - {}^{n-1}\Phi_\phi] \rangle_\square = 0 \quad \forall \delta\phi \in \mathbb{H}^0_{\square,h}, \end{aligned} \tag{A.4}$$

$$\begin{aligned} R_{\mathrm{c},\square}(\phi, c; \delta c) = {} & \Delta t l_\square(\delta c) - \Delta t \langle \boldsymbol{\nabla}[\delta\phi] \cdot \boldsymbol{J}_\mathrm{c} \rangle_\square \\ & - \langle \delta c [\Phi_\mathrm{c} - {}^{n-1}\Phi_\mathrm{c}] \rangle_\square = 0 \quad \forall \delta c \in \mathbb{C}^0_{\square,h}, \end{aligned} \tag{A.5}$$

$$\begin{aligned} (R_{\phi,\square})'_\phi(\phi, c; \delta\phi, \mathrm{d}\phi, 0) = {} & -\langle \delta\phi \Phi'_{\phi\phi}\, \mathrm{d}\phi \rangle_\square - \Delta t \langle \boldsymbol{\nabla}[\delta\phi] \cdot \boldsymbol{Y}_{\phi\phi} \cdot \boldsymbol{\nabla}[\phi]\, \mathrm{d}\phi \rangle_\square \\ & - \Delta t \langle \boldsymbol{\nabla}[\delta\phi] \cdot \boldsymbol{D}_{\phi\phi} \cdot \boldsymbol{\nabla}[\mathrm{d}\phi] \rangle_\square \quad \forall \delta\phi \in \mathbb{H}^0_{\square,h}, \end{aligned} \tag{A.6}$$

$$\begin{aligned} (R_{\phi,\square})'_\mathrm{c}(\phi, c; \delta\phi, 0, \mathrm{d}c) = {} & -\langle \delta\phi \Phi'_{\phi\phi}\, \mathrm{d}\phi \rangle_\square - \Delta t \langle \boldsymbol{\nabla}[\delta\phi] \cdot \boldsymbol{Y}_{\phi \mathrm{c}} \cdot \boldsymbol{\nabla}[c]\, \mathrm{d}c \rangle_\square \\ & - \Delta t \langle \boldsymbol{\nabla}[\delta\phi] \cdot \boldsymbol{D}_{\phi \mathrm{c}} \cdot \boldsymbol{\nabla}[\mathrm{d}c] \rangle_\square \quad \forall \delta\phi \in \mathbb{H}^0_{\square,h}, \end{aligned} \tag{A.7}$$

$$\begin{aligned} (R_{\mathrm{c},\square})'_\mathrm{c}(\phi, c; \delta c, 0, \mathrm{d}c) = {} & -\langle \delta c \Phi'_{\mathrm{cc}}\, \mathrm{d}c \rangle_\square - \Delta t \langle \boldsymbol{\nabla}[\delta c] \cdot \boldsymbol{Y}_{\mathrm{cc}} \cdot \boldsymbol{\nabla}[c]\, \mathrm{d}c \rangle_\square \\ & - \Delta t \langle \boldsymbol{\nabla}[\delta c] \cdot \boldsymbol{D}_{\mathrm{cc}} \cdot \boldsymbol{\nabla}[\mathrm{d}c] \rangle_\square \quad \forall \delta c \in \mathbb{C}^0_{\square,h}, \end{aligned} \tag{A.8}$$

$$\begin{aligned} (R_{\mathrm{c},\square})'_\phi(\phi, c; \delta c, \mathrm{d}\phi, 0) = {} & -\langle \delta\phi \Phi'_{\mathrm{c}\phi}\, \mathrm{d}c \rangle_\square - \Delta t \langle \boldsymbol{\nabla}[\delta c] \cdot \boldsymbol{Y}_{\mathrm{c}\phi} \cdot \boldsymbol{\nabla}[\phi]\, \mathrm{d}\phi \rangle_\square \\ & - \Delta t \langle \boldsymbol{\nabla}[\delta c] \cdot \boldsymbol{D}_{\mathrm{c}\phi} \cdot \boldsymbol{\nabla}[\mathrm{d}\phi] \rangle_\square \quad \forall \delta c \in \mathbb{C}^0_{\square,h}. \end{aligned} \tag{A.9}$$

A.3 Macroscale tangent residuals

The tangent form $(\bar{R})'({}^{n}\bar{z};\delta\bar{z})$ explicitly written out:

$$
\begin{aligned}
(\bar{R}_{\phi})'(\bullet;\delta\bar{\phi},\mathrm{d}\bar{\phi},\mathrm{d}\bar{c}) = &-\int_{\Omega}\delta\bar{\phi}\bar{E}_{\phi\phi}\,\mathrm{d}\bar{\phi}\,\mathrm{d}\Omega-\int_{\Omega}\delta\bar{\phi}\bar{E}_{\phi\mathrm{c}}\,\mathrm{d}\bar{c}\,\mathrm{d}\Omega\\
&-\int_{\Omega}\delta\bar{\phi}\bar{\boldsymbol{B}}_{\phi\phi}\cdot\bar{\boldsymbol{\nabla}}[\mathrm{d}\bar{\phi}]\,\mathrm{d}\Omega-\int_{\Omega}\delta\bar{\phi}\bar{\boldsymbol{B}}_{\phi\mathrm{c}}\cdot\bar{\boldsymbol{\nabla}}[\mathrm{d}\bar{c}]\,\mathrm{d}\Omega\\
&+\int_{\Omega}\bar{\boldsymbol{\nabla}}[\delta\bar{\phi}]\cdot\left[\Delta t\bar{\boldsymbol{Y}}_{\phi\phi}-\bar{\bar{\boldsymbol{E}}}_{\phi\phi}\right]\mathrm{d}\bar{\phi}\,\mathrm{d}\Omega\\
&+\int_{\Omega}\bar{\boldsymbol{\nabla}}[\delta\bar{\phi}]\cdot\left[\Delta t\bar{\boldsymbol{Y}}_{\phi\mathrm{c}}-\bar{\bar{\boldsymbol{E}}}_{\phi\mathrm{c}}\right]\mathrm{d}\bar{c}\,\mathrm{d}\Omega\\
&-\int_{\Omega}\bar{\boldsymbol{\nabla}}[\delta\bar{\phi}]\cdot\left[\Delta t\bar{\boldsymbol{D}}_{\phi\phi}+\bar{\bar{\boldsymbol{B}}}_{\phi\phi}\right]\cdot\bar{\boldsymbol{\nabla}}[\mathrm{d}\bar{\phi}]\,\mathrm{d}\Omega\\
&-\int_{\Omega}\bar{\boldsymbol{\nabla}}[\delta\bar{\phi}]\cdot\left[\Delta t\bar{\boldsymbol{D}}_{\phi\mathrm{c}}+\bar{\bar{\boldsymbol{B}}}_{\phi\mathrm{c}}\right]\cdot\bar{\boldsymbol{\nabla}}[\mathrm{d}\bar{c}]\,\mathrm{d}\Omega,\\
(\bar{R}_{\mathrm{c}})'(\bullet;\delta\bar{c},\mathrm{d}\bar{c},\mathrm{d}\bar{\phi}) = &-\int_{\Omega}\delta\bar{c}\bar{E}_{\mathrm{cc}}\,\mathrm{d}\bar{c}\,\mathrm{d}\Omega-\int_{\Omega}\delta\bar{c}\bar{E}_{\mathrm{c}\phi}\,\mathrm{d}\bar{\phi}\,\mathrm{d}\Omega\\
&-\int_{\Omega}\delta\bar{c}\bar{\boldsymbol{B}}_{\mathrm{cc}}\cdot\bar{\boldsymbol{\nabla}}[\mathrm{d}\bar{c}]\,\mathrm{d}\Omega-\int_{\Omega}\delta\bar{c}\bar{\boldsymbol{B}}_{\mathrm{c}\phi}\cdot\bar{\boldsymbol{\nabla}}[\mathrm{d}\bar{\phi}]\,\mathrm{d}\Omega\\
&+\int_{\Omega}\bar{\boldsymbol{\nabla}}[\delta\bar{c}]\cdot\left[\Delta t\bar{\boldsymbol{Y}}_{\mathrm{cc}}-\bar{\bar{\boldsymbol{E}}}_{\mathrm{cc}}\right]\mathrm{d}\bar{c}\,\mathrm{d}\Omega\\
&+\int_{\Omega}\bar{\boldsymbol{\nabla}}[\delta\bar{c}]\cdot\left[\Delta t\bar{\boldsymbol{Y}}_{\mathrm{c}\phi}-\bar{\bar{\boldsymbol{E}}}_{\mathrm{c}\phi}\right]\mathrm{d}\bar{\phi}\,\mathrm{d}\Omega\\
&-\int_{\Omega}\bar{\boldsymbol{\nabla}}[\delta\bar{c}]\cdot\left[\Delta t\bar{\boldsymbol{D}}_{\mathrm{cc}}+\bar{\bar{\boldsymbol{B}}}_{\mathrm{cc}}\right]\cdot\bar{\boldsymbol{\nabla}}[\mathrm{d}\bar{c}]\,\mathrm{d}\Omega\\
&-\int_{\Omega}\bar{\boldsymbol{\nabla}}[\delta\bar{c}]\cdot\left[\Delta t\bar{\boldsymbol{D}}_{\mathrm{c}\phi}+\bar{\bar{\boldsymbol{B}}}_{\mathrm{c}\phi}\right]\cdot\bar{\boldsymbol{\nabla}}[\mathrm{d}\bar{\phi}]\,\mathrm{d}\Omega.
\end{aligned}
\tag{A.10}
\tag{A.11}
$$

A.4 Macroscale algorithmic tangent operators

First, the components of $\bar{\boldsymbol{J}}$ can be expressed as

$$
\mathrm{d}\bar{J}_i=\mathrm{d}\bar{\boldsymbol{J}}\cdot\boldsymbol{e}_i=\mathrm{d}[\bar{\boldsymbol{J}}\cdot\boldsymbol{e}_i]=\mathrm{d}[\langle\bar{\boldsymbol{J}}\cdot\boldsymbol{e}_i\rangle_{\square}]=-\,\mathrm{d}\left[a_{\square,z}\left(\bullet;\hat{z}^{M(i)}\right)\right]=-a'_{\square,z}\left(\bullet;\hat{z}^{M(i)},\mathrm{d}z\right),
\tag{A.12}
$$

and by inserting the expressions in Eqs. (51) and (52) into Eq. (A.12), we obtain the desired algorithmic operators

$$
\begin{aligned}
(\bar{\boldsymbol{Y}}_{\phi\phi})_i &= -(a_{\phi,\square})'_{\phi}(\bullet; \hat{\phi}^{M(i)}, 1 + \hat{\phi}^{\mathrm{s}}_{\mathrm{d}\phi}, 0) \\
&= \left\langle \boldsymbol{\nabla}\hat{\phi}^{M(i)} \cdot \boldsymbol{Y}_{\phi\phi}[1 + \hat{\phi}^{\mathrm{s}}_{\mathrm{d}\phi}] \right\rangle_{\square} - \left\langle \boldsymbol{\nabla}\hat{\phi}^{M(i)} \cdot \boldsymbol{D}_{\phi\phi} \cdot \boldsymbol{\nabla}\hat{\phi}^{\mathrm{s}}_{\mathrm{d}\phi} \right\rangle_{\square} \qquad \text{(A.13)} \\
&= \langle (\boldsymbol{Y}_{\phi\phi})_i \rangle_{\square} + \langle (\boldsymbol{Y}_{\phi\phi})_i \hat{\phi}^{\mathrm{s}}_{\mathrm{d}\phi} \rangle_{\square} - \langle (\boldsymbol{D}_{\phi\phi} \cdot \boldsymbol{\nabla}\hat{\phi}^{\mathrm{s}}_{\mathrm{d}\phi})_i \rangle_{\square}, \\
(\bar{\boldsymbol{Y}}_{\phi\mathrm{c}})_i &= -(a_{\phi,\square})'_{\mathrm{c}}(\bullet; \hat{c}^{M(i)}, 0, \hat{c}^{\mathrm{s}}_{\mathrm{d}\phi}) \\
&= \left\langle \boldsymbol{\nabla}\hat{\phi}^{M(i)} \cdot \boldsymbol{Y}_{\phi\mathrm{c}}\hat{c}^{\mathrm{s}}_{\mathrm{d}\phi} \right\rangle_{\square} - \left\langle \boldsymbol{\nabla}\hat{\phi}^{M(i)} \cdot \boldsymbol{D}_{\phi\mathrm{c}} \cdot \boldsymbol{\nabla}\hat{c}^{\mathrm{s}}_{\mathrm{d}\phi} \right\rangle_{\square} \qquad \text{(A.14)} \\
&= \langle (\boldsymbol{Y}_{\phi\mathrm{c}})_i \hat{c}^{\mathrm{s}}_{\mathrm{d}\phi} \rangle_{\square} - \langle (\boldsymbol{D}_{\phi\mathrm{c}} \cdot \boldsymbol{\nabla}\hat{c}^{\mathrm{s}}_{\mathrm{d}\phi})_i \rangle_{\square}, \\
(\bar{\boldsymbol{Y}}_{\mathrm{c}\phi})_i &= -(a_{\mathrm{c},\square})'_{\phi}(\bullet; \hat{\phi}^{M(i)}, 0, \hat{\phi}^{\mathrm{s}}_{\mathrm{d}c}) \\
&= \left\langle \boldsymbol{\nabla}\hat{c}^{M(i)} \cdot \boldsymbol{Y}_{\mathrm{c}\phi}\hat{\phi}^{\mathrm{s}}_{\mathrm{d}c} \right\rangle_{\square} - \left\langle \boldsymbol{\nabla}\hat{c}^{M(i)} \cdot \boldsymbol{D}_{\mathrm{c}\phi} \cdot \boldsymbol{\nabla}\hat{\phi}^{\mathrm{s}}_{\mathrm{d}c} \right\rangle_{\square} \qquad \text{(A.15)} \\
&= \langle (\boldsymbol{Y}_{\mathrm{c}\phi})_i \hat{\phi}^{\mathrm{s}}_{\mathrm{d}c} \rangle_{\square} - \langle (\boldsymbol{D}_{\mathrm{c}\phi} \cdot \boldsymbol{\nabla}\hat{\phi}^{\mathrm{s}}_{\mathrm{d}c})_i \rangle_{\square}, \\
(\bar{\boldsymbol{Y}}_{\mathrm{cc}})_i &= -(a_{\mathrm{c},\square})'_{\mathrm{c}}(\bullet; \hat{c}^{M(i)}, 0, 1 + \hat{c}^{\mathrm{s}}_{\mathrm{d}c}) \\
&= \left\langle \boldsymbol{\nabla}\hat{c}^{M(i)} \cdot \boldsymbol{Y}_{\mathrm{c}}[1 + \hat{c}^{\mathrm{s}}_{\mathrm{d}c}] \right\rangle_{\square} - \left\langle \boldsymbol{\nabla}\hat{c}^{M(i)} \cdot \boldsymbol{D}_{\mathrm{c}} \cdot \boldsymbol{\nabla}\hat{c}^{\mathrm{s}}_{\mathrm{d}c} \right\rangle_{\square} \qquad \text{(A.16)} \\
&= \langle (\boldsymbol{Y}_{\mathrm{c}})_i \rangle_{\square} + \langle (\boldsymbol{Y}_{\mathrm{c}})_i \hat{c}^{\mathrm{s}}_{\mathrm{d}c} \rangle_{\square} - \langle (\boldsymbol{D}_{\mathrm{c}} \cdot \boldsymbol{\nabla}\hat{c}^{\mathrm{s}}_{\mathrm{d}c})_i \rangle_{\square},
\end{aligned}
$$

$$
\begin{aligned}
(\bar{\boldsymbol{D}}_{\phi\phi})_{ij} &= (a_{\phi,\square})'_{\phi}(\bullet; \hat{\phi}^{M(i)}, \hat{\phi}^{M(j)} + \hat{\phi}^{s(j)}_{\bar{g}_\phi}, 0) \\
&= \left\langle \boldsymbol{\nabla}\hat{\phi}^{M(i)} \cdot \boldsymbol{D}_{\phi\phi} \cdot \boldsymbol{\nabla}\hat{\phi}^{s(j)}_{\bar{g}_\phi} \right\rangle_{\square} - \left\langle \boldsymbol{\nabla}\hat{\phi}^{M(i)} \cdot \boldsymbol{Y}_{\phi\phi}\hat{\phi}^{s(j)}_{\bar{g}_\phi} \right\rangle_{\square} \\
&= \langle (\boldsymbol{D}_{\phi\phi})_{ij} \rangle_{\square} + \left\langle (\boldsymbol{D}_{\phi\phi} \cdot \boldsymbol{\nabla}\hat{\phi}^{s(j)}_{\bar{g}_\phi})_i \right\rangle_{\square} - \langle (\boldsymbol{Y}_{\phi\phi})_i [x_j - \bar{x}_j] \rangle_{\square} - \left\langle (\boldsymbol{Y}_{\phi\phi})_i \hat{\phi}^{s(j)}_{\bar{g}_\phi} \right\rangle_{\square},
\end{aligned}
\tag{A.17}
$$

$$
\begin{aligned}
(\bar{\boldsymbol{D}}_{\phi\mathrm{c}})_{ij} &= (a_{\phi,\square})'_{\mathrm{c}}(\bullet; \hat{\phi}^{M(i)}, \hat{c}^{s(j)}_{\bar{g}_\phi}, 0) \\
&= \left\langle \boldsymbol{\nabla}\hat{\phi}^{M(i)} \cdot \boldsymbol{D}_{\phi\mathrm{c}} \cdot \boldsymbol{\nabla}\hat{c}^{s(j)}_{\bar{g}_\phi} \right\rangle_{\square} - \left\langle \boldsymbol{\nabla}\hat{\phi}^{M(i)} \cdot \boldsymbol{Y}_{\phi\mathrm{c}}\hat{c}^{s(j)}_{\bar{g}_\phi} \right\rangle_{\square} \\
&= \langle (\boldsymbol{D}_{\phi\mathrm{c}})_{ij} \rangle_{\square} + \left\langle (\boldsymbol{D}_{\phi\mathrm{c}} \cdot \boldsymbol{\nabla}\hat{c}^{s(j)}_{\bar{g}_\phi})_i \right\rangle_{\square} - \langle (\boldsymbol{Y}_{\phi\mathrm{c}})_i [x_j - \bar{x}_j] \rangle_{\square} - \left\langle (\boldsymbol{Y}_{\phi\mathrm{c}})_i \hat{c}^{s(j)}_{\bar{g}_\phi} \right\rangle_{\square},
\end{aligned}
\tag{A.18}
$$

$$
\begin{aligned}
(\bar{\boldsymbol{D}}_{\mathrm{c}\phi})_{ij} &= (a_{\mathrm{c},\square})'_{\phi}(\bullet; \hat{c}^{M(i)}, 0, \hat{\phi}^{s(j)}_{\bar{g}_\mathrm{c}}) \\
&= \left\langle \boldsymbol{\nabla}\hat{c}^{M(i)} \cdot \boldsymbol{D}_{\mathrm{c}\phi} \cdot \boldsymbol{\nabla}\hat{\phi}^{s(j)}_{\bar{g}_\mathrm{c}} \right\rangle_{\square} - \left\langle \boldsymbol{\nabla}\hat{c}^{M(i)} \cdot \boldsymbol{Y}_{\mathrm{c}\phi}\hat{\phi}^{s(j)}_{\bar{g}_\mathrm{c}} \right\rangle_{\square} \\
&= \langle (\boldsymbol{D}_{\mathrm{c}\phi})_{ij} \rangle_{\square} + \left\langle (\boldsymbol{D}_{\mathrm{c}\phi} \cdot \boldsymbol{\nabla}\hat{\phi}^{s(j)}_{\bar{g}_\mathrm{c}})_i \right\rangle_{\square} - \langle (\boldsymbol{Y}_{\mathrm{c}\phi})_i [x_j - \bar{x}_j] \rangle_{\square} - \left\langle (\boldsymbol{Y}_{\mathrm{c}\phi})_i \hat{\phi}^{s(j)}_{\bar{g}_\mathrm{c}} \right\rangle_{\square},
\end{aligned}
\tag{A.19}
$$

$$
\begin{aligned}
(\bar{\boldsymbol{D}}_{\mathrm{cc}})_{ij} &= (a_{\mathrm{c},\square})'_{\mathrm{c}}(\bullet; \hat{c}^{M(i)}, 0, \hat{c}^{M(j)} + \hat{c}^{s(j)}_{\mathrm{c}}) \\
&= \left\langle \boldsymbol{\nabla}\hat{c}^{M(i)} \cdot \boldsymbol{D}_{\mathrm{cc}} \cdot \boldsymbol{\nabla}\hat{c}^{s(j)}_{\mathrm{c}} \right\rangle_{\square} - \left\langle \boldsymbol{\nabla}\hat{c}^{M(i)} \cdot \boldsymbol{Y}_{\mathrm{cc}}\hat{c}^{s(j)}_{\mathrm{c}} \right\rangle_{\square} \\
&= \langle (\boldsymbol{D}_{\mathrm{cc}})_{ij} \rangle_{\square} + \left\langle (\boldsymbol{D}_{\mathrm{cc}} \cdot \boldsymbol{\nabla}\hat{c}^{s(j)}_{\mathrm{c}})_i \right\rangle_{\square} - \langle (\boldsymbol{Y}_{\mathrm{cc}})_i [x_j - \bar{x}_j] \rangle_{\square} - \left\langle (\boldsymbol{Y}_{\mathrm{cc}})_i \hat{c}^{s(j)}_{\mathrm{c}} \right\rangle_{\square}.
\end{aligned}
\tag{A.20}
$$

Next, we consider the linearization of $\bar{\Phi}$ and $\bar{\bar{\mathbf{\Phi}}}$. From Eq. $(22)_2$ we obtain

$$\mathrm{d}\bar{\Phi}_\phi = \mathrm{d}\langle\Phi_\phi\rangle_\square = \langle\Phi'_{\phi\phi}\,\mathrm{d}\phi\rangle_\square + \langle\Phi'_{\phi\mathrm{c}}\,\mathrm{d}c\rangle_\square, \tag{A.21}$$

$$\mathrm{d}\bar{\Phi}_\mathrm{c} = \mathrm{d}\langle\Phi_\mathrm{c}\rangle_\square = \langle\Phi'_{\mathrm{cc}}\,\mathrm{d}c\rangle_\square + \langle\Phi'_{\mathrm{c}\phi}\,\mathrm{d}\phi\rangle_\square, \tag{A.22}$$

and by inserting the representations of $\mathrm{d}\phi$ and $\mathrm{d}c$ from Eqs. (51) and (52) into Eqs. (A.21) and (A.22), we identify the tangent operators

$$\bar{E}_{\phi\phi} = \left\langle \Phi'_{\phi\phi}[1+\hat{\phi}^{s(i)}_{\bar{\phi}}]\right\rangle_\square = \langle\Phi'_{\phi\phi}\rangle_\square + \left\langle \Phi'_{\phi\phi}\hat{\phi}^{s(i)}_{\bar{\phi}}\right\rangle_\square, \tag{A.23}$$

$$\bar{E}_{\phi\mathrm{c}} = \left\langle \Phi'_{\phi\mathrm{c}}\hat{c}^{s(i)}_{\bar{\phi}}\right\rangle_\square, \tag{A.24}$$

$$\bar{E}_{\mathrm{cc}} = \left\langle \Phi'_{\mathrm{cc}}[1+\hat{c}^{s(i)}_{\bar{\mathrm{c}}}]\right\rangle_\square = \langle\Phi'_{\mathrm{cc}}\rangle_\square + \left\langle \Phi'_{\mathrm{cc}}\hat{c}^{s(i)}_{\bar{\mathrm{c}}}\right\rangle_\square, \tag{A.25}$$

$$\bar{E}_{\mathrm{c}\phi} = \left\langle \Phi'_{\mathrm{c}\phi}\hat{\phi}^{s(i)}_{\bar{\mathrm{c}}}\right\rangle_\square, \tag{A.26}$$

$$(\bar{\boldsymbol{B}}_{\phi\phi})_i = \left\langle \Phi'_{\phi\phi}\left[\hat{\phi}^{M(i)}+\hat{\phi}^{s(i)}_{\bar{g}_\phi}\right]\right\rangle_\square = \langle\Phi'_{\phi\phi}[x_i-\bar{x}_i]\rangle_\square + \left\langle \Phi'_{\phi\phi}\hat{\phi}^{s(i)}_{\bar{g}_\phi}\right\rangle_\square, \tag{A.27}$$

$$(\bar{\boldsymbol{B}}_{\phi\mathrm{c}})_i = \left\langle \Phi'_{\phi\mathrm{c}}\hat{c}^{s(i)}_{\bar{g}_\phi}\right\rangle_\square, \tag{A.28}$$

$$(\bar{\boldsymbol{B}}_{\mathrm{c}\phi})_i = \left\langle \Phi'_{\mathrm{c}\phi}\hat{\phi}^{s(i)}_{\bar{g}_\mathrm{c}}\right\rangle_\square, \tag{A.29}$$

$$(\bar{\boldsymbol{B}}_{\mathrm{cc}})_i = \left\langle \Phi'_{\mathrm{cc}}\left[\hat{c}^{M(i)}+\hat{c}^{s(i)}_{\bar{g}_\mathrm{c}}\right]\right\rangle_\square = \langle\Phi'_{\mathrm{cc}}[x_i-\bar{x}_i]\rangle_\square + \left\langle \Phi'_{\mathrm{cc}}\hat{c}^{s(i)}_{\bar{g}_\mathrm{c}}\right\rangle_\square. \tag{A.30}$$

Finally, from Eq. (23) we obtain generically that

$$(\mathrm{d}\bar{\bar{\boldsymbol{\Phi}}})_i = \mathrm{d}\langle \Phi[x_i - \bar{x}_i]\,\mathrm{d}z\rangle_\square = \mathrm{d}\Big\langle \Phi \hat{z}^{M(i)}\,\mathrm{d}z\Big\rangle_\square = \Big\langle \Phi' \hat{z}^{M(i)}\,\mathrm{d}z\Big\rangle_\square = \langle \Phi'[x_i - \bar{x}_i]\,\mathrm{d}z\rangle_\square, \tag{A.31}$$

and upon inserting the representations of $\mathrm{d}\phi$ and $\mathrm{d}c$ from Eqs. (51) and (52) into Eq. (A.31), we identify the tangent operators

$$\begin{aligned}(\bar{\bar{\boldsymbol{E}}}_{\phi\phi})_i &= \Big\langle \Phi'_{\phi\phi}\hat{\phi}^{M(i)}[1 + \hat{\phi}^{\mathrm{s}}_{\bar{\phi}}]\Big\rangle_\square \\ &= \langle \Phi'_{\phi\phi}[x_i - \bar{x}_i]\rangle_\square + \Big\langle \Phi'_{\phi\phi}[x_i - \bar{x}_i]\hat{\phi}^{s(i)}_{\bar{\phi}}\Big\rangle_\square,\end{aligned} \tag{A.32}$$

$$(\bar{\bar{\boldsymbol{E}}}_{\phi\mathrm{c}})_i = \Big\langle \Phi'_{\phi\mathrm{c}}\hat{\phi}^{M(i)}\hat{c}^{\mathrm{s}}_{\bar{\phi}}\Big\rangle_\square + \Big\langle \Phi'_{\phi\mathrm{c}}[x_i - \bar{x}_i]\hat{c}^{s(i)}_{\bar{\phi}}\Big\rangle_\square, \tag{A.33}$$

$$(\bar{\bar{\boldsymbol{E}}}_{\mathrm{c}\phi})_i = \Big\langle \Phi'_{\mathrm{c}\phi}\hat{c}^{M(i)}\hat{\phi}^{\mathrm{s}}_{\bar{\mathrm{c}}}\Big\rangle_\square + \Big\langle \Phi'_{\mathrm{c}\phi}[x_i - \bar{x}_i]\hat{\phi}^{s(i)}_{\bar{\mathrm{c}}}\Big\rangle_\square, \tag{A.34}$$

$$\begin{aligned}(\bar{\bar{\boldsymbol{E}}}_{\mathrm{cc}})_i &= \Big\langle \Phi'_{\mathrm{cc}}\hat{c}^{M(i)}[1 + \hat{c}^{\mathrm{s}}_{\bar{\mathrm{c}}}]\Big\rangle_\square \\ &= \langle \Phi'_{\mathrm{cc}}[x_i - \bar{x}_i]\rangle_\square + \Big\langle \Phi'_{\mathrm{cc}}[x_i - \bar{x}_i]\hat{c}^{s(i)}_{\bar{\mathrm{c}}}\Big\rangle_\square,\end{aligned} \tag{A.35}$$

$$\begin{aligned}(\bar{\bar{\boldsymbol{B}}}_{\phi\phi})_{ij} &= \Big\langle \Phi'_{\phi\phi}\hat{\phi}^{M(i)}\Big[\hat{\phi}^{M(j)} + \hat{\phi}^{s(j)}_{\bar{g}_\phi}\Big]\Big\rangle_\square \\ &= \langle \Phi_{\phi\phi}[x_i - \bar{x}_i][x_j - \bar{x}_j]\rangle_\square + \Big\langle \Phi'_{\phi\phi}[x_i - \bar{x}_i]\hat{\phi}^{s(j)}_{\bar{g}_\phi}\Big\rangle_\square,\end{aligned} \tag{A.36}$$

$$(\bar{\bar{\boldsymbol{B}}}_{\phi\mathrm{c}})_i = \Big\langle \Phi'_{\phi\mathrm{c}}[x_j - \bar{x}_j]\hat{c}^{s(i)}_{\bar{g}_\phi}\Big\rangle_\square \tag{A.37}$$

$$(\bar{\bar{\boldsymbol{B}}}_{\mathrm{c}\phi})_i = \Big\langle \Phi'_{\mathrm{c}\phi}[x_j - \bar{x}_j]\hat{\phi}^{s(i)}_{\bar{g}_\mathrm{c}}\Big\rangle_\square, \tag{A.38}$$

$$\begin{aligned}(\bar{\bar{\boldsymbol{B}}}_{\mathrm{cc}})_{ij} &= \Big\langle \Phi'_{\mathrm{cc}}\hat{c}^{M(i)}\Big[\hat{c}^{M(j)} + \hat{c}^{s(j)}_{\bar{g}_\mathrm{c}}\Big]\Big\rangle_\square \\ &= \langle \Phi_{\mathrm{cc}}[x_i - \bar{x}_i][x_j - \bar{x}_j]\rangle_\square + \Big\langle \Phi'_{\mathrm{cc}}[x_i - \bar{x}_i]\hat{c}^{s(j)}_{\bar{g}_\mathrm{c}}\Big\rangle_\square.\end{aligned} \tag{A.39}$$

Remark 8 *Generically, although Φ is assumed not to depend on $\boldsymbol{\nabla} z$, i.e. $\boldsymbol{B} \overset{\mathrm{def}}{=} \partial\Phi/\partial(\boldsymbol{\nabla} z) = \boldsymbol{0}$, it appears that a "nonlocal" contribution is obtained upon carrying out the homogenization in the sense that, still, $\bar{\boldsymbol{B}} \neq \boldsymbol{0}$. Likewise, even if we had employed a simplified constitutive law such that $\boldsymbol{J}$ does not depend on z, i.e. $\boldsymbol{Y} = \boldsymbol{0}$, there would still be a "nonlocal" contribution to $\bar{\boldsymbol{Y}} \neq \boldsymbol{0}$ from the fluctuation field.* □

A.5 Sensitivity equations

(i) Sensitivity w.r.t. $\bar{\phi}$:

Solve for $\hat{\phi}^{\mathrm{s}}_{\bar{\phi}} \overset{\mathrm{def}}{=} {}^{n}\hat{\phi}^{\mathrm{s}}_{\bar{\phi}} \in {}^{0}_{\square,h}$ and $\hat{c}^{\mathrm{s}}_{\bar{\phi}} \overset{\mathrm{def}}{=} {}^{n}\hat{c}^{\mathrm{s}}_{\bar{\phi}} \in \mathbb{C}^{0}_{\square,h}$ from

$$
\begin{aligned}
&(R_{\phi,\square})'_{\phi}(\phi, c; \delta\phi, 1 + \hat{\phi}^{\mathrm{s}}_{\bar{\phi}}, 0) + (R_{\phi,\square})'_{\mathrm{c}}(\phi, c; \delta\phi, 0, \hat{c}^{\mathrm{s}}_{\bar{\phi}}) = 0 \\
&\Leftrightarrow \\
&\langle \delta\phi \Phi'_{\phi\phi} \hat{\phi}^{\mathrm{s}}_{\bar{\phi}} \rangle_{\square} + \langle \delta\phi \Phi'_{\phi\mathrm{c}} \hat{c}^{\mathrm{s}}_{\bar{\phi}} \rangle_{\square} + \Delta t \left\langle \boldsymbol{\nabla}[\delta\phi] \cdot \boldsymbol{Y}_{\phi\phi} \hat{\phi}^{\mathrm{s}}_{\bar{\phi}} \right\rangle_{\square} + \Delta t \langle \boldsymbol{\nabla}[\delta\phi] \cdot \boldsymbol{D}_{\phi\phi} \cdot \boldsymbol{\nabla}[\hat{\phi}^{\mathrm{s}}_{\bar{\phi}}] \rangle_{\square} \\
&+ \Delta t \left\langle \boldsymbol{\nabla}[\delta\phi] \cdot \boldsymbol{Y}_{\phi\mathrm{c}} \hat{c}^{\mathrm{s}}_{\bar{\phi}} \right\rangle_{\square} + \Delta t \langle \boldsymbol{\nabla}[\delta\phi] \cdot \boldsymbol{D}_{\phi\mathrm{c}} \cdot \boldsymbol{\nabla}[\hat{c}^{\mathrm{s}}_{\bar{\phi}}] \rangle_{\square} \\
&= -\langle \delta\phi \Phi'_{\phi\phi} \rangle_{\square} - \Delta t \left\langle \boldsymbol{\nabla}[\delta\phi] \cdot \boldsymbol{Y}_{\phi\phi} \right\rangle_{\square} \quad \forall \hat{\phi}^{\mathrm{s}} \in {}^{0}_{\square,h},
\end{aligned}
\tag{A.40}
$$

$$
\begin{aligned}
&(R_{\mathrm{c},\square})'_{\phi}(\phi, c; \delta\phi, 1 + \hat{\phi}^{\mathrm{s}}_{\bar{\phi}}, 0) + (R_{\mathrm{c},\square})'_{\mathrm{c}}(\phi, c; \delta\phi, 0, \hat{c}^{\mathrm{s}}_{\bar{\phi}}) = 0 \\
&\Leftrightarrow \\
&\langle \delta\phi \Phi'_{\mathrm{c}\phi} \hat{\phi}^{\mathrm{s}}_{\bar{\phi}} \rangle_{\square} + \langle \delta\phi \Phi'_{\mathrm{cc}} \hat{c}^{\mathrm{s}}_{\bar{\phi}} \rangle_{\square} + \Delta t \left\langle \boldsymbol{\nabla}[\delta\phi] \cdot \boldsymbol{Y}_{\mathrm{c}\phi} \hat{\phi}^{\mathrm{s}}_{\bar{\phi}} \right\rangle_{\square} + \Delta t \langle \boldsymbol{\nabla}[\delta\phi] \cdot \boldsymbol{D}_{\mathrm{c}\phi} \cdot \boldsymbol{\nabla}[\hat{\phi}^{\mathrm{s}}_{\bar{\phi}}] \rangle_{\square} \\
&+ \Delta t \left\langle \boldsymbol{\nabla}[\delta\phi] \cdot \boldsymbol{Y}_{\mathrm{cc}} \hat{c}^{\mathrm{s}}_{\bar{\phi}} \right\rangle_{\square} + \Delta t \langle \boldsymbol{\nabla}[\delta\phi] \cdot \boldsymbol{D}_{\mathrm{cc}} \cdot \boldsymbol{\nabla}[\hat{c}^{\mathrm{s}}_{\bar{\phi}}] \rangle_{\square} \\
&= -\langle \delta\phi \Phi'_{\mathrm{c}\phi} \rangle_{\square} - \Delta t \left\langle \boldsymbol{\nabla}[\delta\phi] \cdot \boldsymbol{Y}_{\mathrm{c}\phi} \right\rangle_{\square} \quad \forall \hat{\phi}^{\mathrm{s}} \in {}^{0}_{\square,h}.
\end{aligned}
\tag{A.41}
$$

(ii) Sensitivity w.r.t. $\bar{c}$:

Solve for $\hat{\phi}^{\mathrm{s}}_{\bar{\mathrm{c}}} \overset{\mathrm{def}}{=} {}^{n}\hat{\phi}^{\mathrm{s}}_{\bar{\mathrm{c}}} \in {}^{0}_{\square,h}$ and $\hat{c}^{\mathrm{s}}_{\bar{\mathrm{c}}} \overset{\mathrm{def}}{=} {}^{n}\hat{c}^{\mathrm{s}}_{\bar{\mathrm{c}}} \in \mathbb{C}^{0}_{\square,h}$ from

$$
\begin{aligned}
&(R_{\phi,\square})'_{\phi}(\phi, c; \delta c, \hat{\phi}^{\mathrm{s}}_{\bar{\mathrm{c}}}, 0) + (R_{\phi,\square})'_{\mathrm{c}}(\phi, c; \delta c, 0, \hat{c}^{\mathrm{s}}_{\bar{\mathrm{c}}}) = 0 \\
&\Leftrightarrow \\
&\langle \delta c \Phi'_{\phi\phi} \hat{\phi}^{\mathrm{s}}_{\bar{\mathrm{c}}} \rangle_{\square} + \langle \delta c \Phi'_{\phi\mathrm{c}} \hat{c}^{\mathrm{s}}_{\bar{\mathrm{c}}} \rangle_{\square} + \Delta t \left\langle \boldsymbol{\nabla}[\delta c] \cdot \boldsymbol{Y}_{\phi\phi} \hat{\phi}^{\mathrm{s}}_{\bar{\mathrm{c}}} \right\rangle_{\square} + \Delta t \langle \boldsymbol{\nabla}[\delta c] \cdot \boldsymbol{D}_{\phi\phi} \cdot \boldsymbol{\nabla}[\hat{\phi}^{\mathrm{s}}_{\bar{\mathrm{c}}}] \rangle_{\square} \\
&+ \Delta t \left\langle \boldsymbol{\nabla}[\delta c] \cdot \boldsymbol{Y}_{\phi\mathrm{c}} \hat{c}^{\mathrm{s}}_{\bar{\mathrm{c}}} \right\rangle_{\square} + \Delta t \langle \boldsymbol{\nabla}[\delta c] \cdot \boldsymbol{D}_{\phi\mathrm{c}} \cdot \boldsymbol{\nabla}[\hat{c}^{\mathrm{s}}_{\bar{\mathrm{c}}}] \rangle_{\square} \\
&= -\langle \delta c \Phi'_{\phi\phi} \rangle_{\square} - \Delta t \left\langle \boldsymbol{\nabla}[\delta c] \cdot \boldsymbol{Y}_{\phi\phi} \right\rangle_{\square} \quad \forall \hat{\phi}^{\mathrm{s}} \in {}^{0}_{\square,h},
\end{aligned}
\tag{A.42}
$$

$$
\begin{aligned}
&(R_{\mathrm{c},\square})'_{\phi}(\phi, c; \delta c, 1 + \hat{\phi}^{\mathrm{s}}_{\bar{\mathrm{c}}}, 0) + (R_{\mathrm{c},\square})'_{\mathrm{c}}(\phi, c; \delta c, 0, \hat{c}^{\mathrm{s}}_{\bar{\mathrm{c}}}) = 0 \\
&\Leftrightarrow \\
&\langle \delta c \Phi'_{\mathrm{c}\phi} \hat{\phi}^{\mathrm{s}}_{\bar{\mathrm{c}}} \rangle_{\square} + \langle \delta c \Phi'_{\mathrm{cc}} \hat{c}^{\mathrm{s}}_{\bar{\mathrm{c}}} \rangle_{\square} + \Delta t \left\langle \boldsymbol{\nabla}[\delta c] \cdot \boldsymbol{Y}_{\mathrm{c}\phi} \hat{\phi}^{\mathrm{s}}_{\bar{\mathrm{c}}} \right\rangle_{\square} + \Delta t \langle \boldsymbol{\nabla}[\delta c] \cdot \boldsymbol{D}_{\mathrm{c}\phi} \cdot \boldsymbol{\nabla}[\hat{\phi}^{\mathrm{s}}_{\bar{\mathrm{c}}}] \rangle_{\square} \\
&+ \Delta t \left\langle \boldsymbol{\nabla}[\delta c] \cdot \boldsymbol{Y}_{\mathrm{cc}} \hat{c}^{\mathrm{s}}_{\bar{\mathrm{c}}} \right\rangle_{\square} + \Delta t \langle \boldsymbol{\nabla}[\delta c] \cdot \boldsymbol{D}_{\mathrm{cc}} \cdot \boldsymbol{\nabla}[\hat{c}^{\mathrm{s}}_{\bar{\mathrm{c}}}] \rangle_{\square} \\
&= -\langle \delta c \Phi'_{\mathrm{c}\phi} \rangle_{\square} - \Delta t \left\langle \boldsymbol{\nabla}[\delta c] \cdot \boldsymbol{Y}_{\mathrm{c}\phi} \right\rangle_{\square} \quad \forall \hat{\phi}^{\mathrm{s}} \in {}^{0}_{\square,h}.
\end{aligned}
\tag{A.43}
$$

(iii) Sensitivity w.r.t. $\bar{g}_\phi$:

Solve for $\hat{\phi}^{\mathrm{s}}_{\bar{g}_\phi} \overset{\text{def}}{=} {}^{n}\hat{\phi}^{\mathrm{s}}_{\bar{g}_\phi} \in {}^{0}_{\square,h}$ and $\hat{c}^{\mathrm{s}}_{\bar{g}_\phi} \overset{\text{def}}{=} {}^{n}\hat{c}^{\mathrm{s}}_{\bar{g}_\phi} \in {}^{0}_{\square,h}$ from

$$
\begin{aligned}
&(R_{\phi,\square})'_\phi(\phi, c; \delta\phi, \hat{\phi}^{\mathrm{M}} + \hat{\phi}^{\mathrm{s}}_{\bar{g}_\phi}, 0) + (R_{\phi,\square})'_{\mathrm{c}}(\phi, c, \delta\phi, 0, \hat{c}^{\mathrm{s}}_{\bar{g}_\phi}) = 0 \\
&\Leftrightarrow \\
&\left\langle \delta\phi \Phi'_{\phi\phi} \hat{\phi}^{s(i)}_{\bar{g}_\phi} \right\rangle_\square + \left\langle \delta\phi \Phi'_{\phi\mathrm{c}} \hat{c}^{s(i)}_{\bar{g}_\phi} \right\rangle_\square + \Delta t \left\langle \boldsymbol{\nabla}[\delta\phi] \cdot \boldsymbol{Y}_{\phi\phi} \hat{\phi}^{s(i)}_{\bar{g}_\phi} \right\rangle_\square + \Delta t \left\langle \boldsymbol{\nabla}[\delta\phi] \cdot \boldsymbol{D}_{\phi\phi} \cdot \boldsymbol{\nabla}[\hat{\phi}^{\mathrm{s}}_{\bar{g}_\phi}] \right\rangle_\square \\
&+ \Delta t \left\langle \boldsymbol{\nabla}[\delta\phi] \cdot \boldsymbol{Y}_{\phi\mathrm{c}} \hat{c}^{s(i)}_{\bar{g}_\phi} \right\rangle_\square + \Delta t \left\langle \boldsymbol{\nabla}[\delta\phi] \cdot \boldsymbol{D}_{\phi\mathrm{c}} \cdot \boldsymbol{\nabla}[\hat{c}^{s(i)}_{\bar{g}_\phi}] \right\rangle_\square \\
&= -\langle \delta\phi \Phi'_{\phi\phi}[x_i - \bar{x}_i] \rangle_\square - \Delta t \left\langle \boldsymbol{\nabla}[\delta\phi] \cdot \boldsymbol{Y}_{\phi\phi}[x_i - \bar{x}_i] \right\rangle_\square - \Delta t \left\langle \boldsymbol{\nabla}[\delta\phi] \cdot \boldsymbol{D}_{\phi\phi} \cdot \boldsymbol{e}_i \right\rangle_\square, \quad \forall \delta\phi \in \mathbb{H}^0_{\square,h},
\end{aligned}
\tag{A.44}
$$

$$
\begin{aligned}
&(R_{\mathrm{c},\square})'_\phi(\phi, c; \delta\phi, \hat{\phi}^{\mathrm{M}} + \hat{\phi}^{\mathrm{s}}_{\bar{g}_\phi}, 0) + (R_{\mathrm{c},\square})'_{\mathrm{c}}(\phi, c, \delta\phi, 0, \hat{c}^{\mathrm{s}}_{\bar{g}_\phi}) = 0 \\
&\Leftrightarrow \\
&\left\langle \delta\phi \Phi'_{\mathrm{c}\phi} \hat{\phi}^{s(i)}_{\bar{g}_\phi} \right\rangle_\square + \left\langle \delta\phi \Phi'_{\mathrm{cc}} \hat{c}^{s(i)}_{\bar{g}_\phi} \right\rangle_\square + \Delta t \left\langle \boldsymbol{\nabla}[\delta\phi] \cdot \boldsymbol{Y}_{\mathrm{c}\phi} \hat{\phi}^{s(i)}_{\bar{g}_\phi} \right\rangle_\square + \Delta t \left\langle \boldsymbol{\nabla}[\delta\phi] \cdot \boldsymbol{D}_{\mathrm{c}\phi} \cdot \boldsymbol{\nabla}[\hat{\phi}^{\mathrm{s}}_{\bar{g}_\phi}] \right\rangle_\square \\
&+ \Delta t \left\langle \boldsymbol{\nabla}[\delta\phi] \cdot \boldsymbol{Y}_{\mathrm{cc}} \hat{c}^{s(i)}_{\bar{g}_\phi} \right\rangle_\square + \Delta t \left\langle \boldsymbol{\nabla}[\delta\phi] \cdot \boldsymbol{D}_{\mathrm{cc}} \cdot \boldsymbol{\nabla}[\hat{c}^{s(i)}_{\bar{g}_\phi}] \right\rangle_\square \\
&= -\langle \delta\phi \Phi'_{\mathrm{c}\phi}[x_i - \bar{x}_i] \rangle_\square - \Delta t \left\langle \boldsymbol{\nabla}[\delta\phi] \cdot \boldsymbol{Y}_{\mathrm{c}\phi}[x_i - \bar{x}_i] \right\rangle_\square - \Delta t \left\langle \boldsymbol{\nabla}[\delta\phi] \cdot \boldsymbol{D}_{\mathrm{c}\phi} \cdot \boldsymbol{e}_i \right\rangle_\square, \quad \forall \delta\phi \in \mathbb{H}^0_{\square,h}.
\end{aligned}
\tag{A.45}
$$

(iv) Sensitivity w.r.t. $\bar{g}_c$:
Solve for $\hat{\phi}^s_{\bar{g}_\phi} \overset{\text{def}}{=} {}^n\hat{\phi}^s_{\bar{g}_\phi} \in {}^0_{\square,h}$ and $\hat{c}^s_{\bar{g}_\phi} \overset{\text{def}}{=} {}^n\hat{c}^s_{\bar{g}_\phi} \in {}^0_{\square,h}$ from

$$
\begin{aligned}
&(R_{\phi,\square})'_\phi(\phi, c; \delta\phi, \hat{\phi}^M + \hat{\phi}^s_{\bar{g}_c}, 0) + (R_{\phi,\square})'_c(\phi, c, \delta\phi, 0, \hat{c}^s_{\bar{g}_c}) = 0 \\
&\Leftrightarrow \\
&\left\langle \delta\phi \Phi'_{\phi\phi} \hat{\phi}^{s(i)}_{\bar{g}_c} \right\rangle_\square + \left\langle \delta\phi \Phi'_{\phi c} \hat{c}^{s(i)}_{\bar{g}_c} \right\rangle_\square + \Delta t \left\langle \boldsymbol{\nabla}[\delta\phi] \cdot \boldsymbol{Y}_{\phi\phi} \hat{\phi}^{s(i)}_{\bar{g}_c} \right\rangle_\square + \Delta t \left\langle \boldsymbol{\nabla}[\delta\phi] \cdot \boldsymbol{D}_{\phi\phi} \cdot \boldsymbol{\nabla}[\hat{\phi}^s_{\bar{g}_c}] \right\rangle_\square \\
&+ \Delta t \left\langle \boldsymbol{\nabla}[\delta\phi] \cdot \boldsymbol{Y}_{\phi c} \hat{c}^{s(i)}_{\bar{g}_c} \right\rangle_\square + \Delta t \left\langle \boldsymbol{\nabla}[\delta\phi] \cdot \boldsymbol{D}_{\phi c} \cdot \boldsymbol{\nabla}[\hat{c}^{s(i)}_{\bar{g}_c}] \right\rangle_\square \\
&= -\langle \delta\phi \Phi'_{\phi\phi}[x_i - \bar{x}_i] \rangle_\square - \Delta t \left\langle \boldsymbol{\nabla}[\delta\phi] \cdot \boldsymbol{Y}_{\phi\phi}[x_i - \bar{x}_i] \right\rangle_\square - \Delta t \left\langle \boldsymbol{\nabla}[\delta\phi] \cdot \boldsymbol{D}_{\phi\phi} \cdot \boldsymbol{e}_i \right\rangle_\square, \quad \forall \delta\phi \in \mathbb{H}^0_{\square,h},
\end{aligned}
\tag{A.46}
$$

$$
\begin{aligned}
&(R_{c,\square})'_\phi(\phi, c; \delta\phi, \hat{\phi}^M + \hat{\phi}^s_{\bar{g}_c}, 0) + (R_{c,\square})'_c(\phi, c, \delta\phi, 0, \hat{c}^s_{\bar{g}_c}) = 0 \\
&\Leftrightarrow \\
&\left\langle \delta\phi \Phi'_{c\phi} \hat{\phi}^{s(i)}_{\bar{g}_c} \right\rangle_\square + \left\langle \delta\phi \Phi'_{cc} \hat{c}^{s(i)}_{\bar{g}_c} \right\rangle_\square + \Delta t \left\langle \boldsymbol{\nabla}[\delta\phi] \cdot \boldsymbol{Y}_{c\phi} \hat{\phi}^{s(i)}_{\bar{g}_c} \right\rangle_\square + \Delta t \left\langle \boldsymbol{\nabla}[\delta\phi] \cdot \boldsymbol{D}_{c\phi} \cdot \boldsymbol{\nabla}[\hat{\phi}^s_{\bar{g}_c}] \right\rangle_\square \\
&+ \Delta t \left\langle \boldsymbol{\nabla}[\delta\phi] \cdot \boldsymbol{Y}_{cc} \hat{c}^{s(i)}_{\bar{g}_c} \right\rangle_\square + \Delta t \left\langle \boldsymbol{\nabla}[\delta\phi] \cdot \boldsymbol{D}_{cc} \cdot \boldsymbol{\nabla}[\hat{c}^{s(i)}_{\bar{g}_c}] \right\rangle_\square \\
&= -\langle \delta\phi \Phi'_{c\phi}[x_i - \bar{x}_i] \rangle_\square - \Delta t \left\langle \boldsymbol{\nabla}[\delta\phi] \cdot \boldsymbol{Y}_{c\phi}[x_i - \bar{x}_i] \right\rangle_\square - \Delta t \left\langle \boldsymbol{\nabla}[\delta\phi] \cdot \boldsymbol{D}_{c\phi} \cdot \boldsymbol{e}_i \right\rangle_\square, \quad \forall \delta\phi \in \mathbb{H}^0_{\square,h}.
\end{aligned}
\tag{A.47}
$$

Remark 9 *Each pair of equations in (i) to (iv) are coupled.*

Acknowledgments

This research was financially supported by The Swedish Research Council, which is gratefully acknowledged.

References

Ababneh, A. (2002). "The coupled effect of moisture diffusion chloride penetration and freezing-thawing on concrete." Ph.D. thesis, University of Colorado at Boulder, Department of Civil, Environmental and Architectural Engineering,

Ababneh, A., Benboudjema, F., and Xi, Y. (2003). "Chloride penetration in nonsaturated concrete." *J. Mater. Civ. Eng.*, 15(2), 183–191.

Bažant, Z. P. and Najjar, L. J. (1972). "Nonlinear water diffusion in nonsaturated concrete." *Mater. Struct.*, 5(1), 3–20.

Caballero, A., Lopez, C., and Carol, I. (2006). "3D meso-structural analysis of concrete specimens under uniaxial tension." *Comput. Methods Appl. Mech. Engrg.*, 195(52), 7182–7195.

Eriksson, K., Estep, D., Hansbo, P., and Johnson, C. (1996). *Computational differential equations*. Studentlitteratur.

Garboczi, E. (1998). "Multiscale Analytical/Numerical Theory of the Diffusivity of Concrete." *Adv. Cem. Based Mater.*, 8(2), 77–88.

Hain, M. and Wriggers, P. (2007). "Numerical homogenization of hardened cement paste." *Computational Mechanics*, 42(2), 197–212.

Hain, M. and Wriggers, P. (2008). "Computational homogenization of micro-structural damage due to frost in hardened cement paste." *Finite. Elem. Anal. Des.*, 44(5), 233–244.

Koniorczyk, M. and Wojciechowski, M. (2009). "Influence of salt on desorption isotherm and hygral state of cement mortar – Modelling using neural networks." *Constr Build Mater.*, 23(9), 2988–2996.

Larsson, F., Runesson, K., and Su, F. (2009). "Variationally consistent computational homogenization of transient heat flow." *Int. J. Numer. Meth. Eng.*, 81(13), 1659–1686.

Li, L.-Y., Xia, J., and Lin, S.-S. (2011). "A multi-phase model for predicting the effective diffusion coefficient of chlorides in concrete." *Constr Build Mater.*

Mehta, P. K. and Monteiro, P. J. M. (2006). *Concrete: Microstructure, Properties and Materials*. McGraw-Hill Professional.

Nemat-Nasser, S. and Hori, M. (1999). *Micromechanics: Overall Properties of Heterogeneous Materials*. Elsevier.

Nilenius, F., Larsson, F., Lundgren, K., and Runesson, K. (2012). "Macroscopic diffusivity in concrete determined by computational homogenization." *Int. J. Numer. Anal. Meth. Geomech.*

Özdemir, I., Brekelmans, W., and Geers, M. (2008). "FE^2 computational homogenization for the thermo-mechanical analysis of heterogeneous solids." *Comput. Methods Appl. Mech. Engrg.*, 198(3-4), 602–613.

Rossignolo, J. A. (2007). "Effect of silica fume and SBR latex on the pasteaggregate interfacial transition zone." *Materials Research*, 10(1), 83–86.

Stankowski, T. (1990). "Numerical simulation of progressive failure in particle composites." Ph.D. thesis, C.E.A.E. Department, University of Colorado, Boulder,

Suwito, A., Cai, X.-C., and Xi, Y. (2006). "Parallel Finite Element Method for Coupled Chloride and Moisture Diffusion in Concrete." *Int. J. Numer. Anal. Model.*, 3(4), 481–503.

Tang, L. and Nilsson, L. O. (1993). "Chloride Binding Capacity and Binding Isotherms of OPC Pastes and Mortars." *Cement Concr. Res.*, 23, 247–253.

Černý, R. (2004). "Experimental analysis of coupled water and chloride transport in cement mortar." *Cement and Concrete Comp.*, 26(6), 705–715.

Černý, R. and Rovnaníková, P. (2002). *Transport processes in concrete*. Spon Press.

Xi, Y. and Bažant, Z. P. (1999). "Modeling Chloride Penetration in Saturated Concrete." *J. Mater. Civ. Eng.*, 11(1), 58–66.

Xi, Y., Bažant, Z. P., Molina, L., and Jennings, M. (1994). "Moisture diffusion in cementitious materials: Moisture capacity and diffusivity." *Adv. Cem. Based Mater.*, 1(6), 258–266.

Yuan, Z. and Fish, J. (2008). "Toward realization of computational homogenization in practice." *Int. J. Numer. Meth. Eng.*, 73(3), 361–380.

Zeng, Y. (2007). "Modeling of chloride diffusion in hetero-structured concretes by finite element method." *Cement and Concrete Comp.*, 29(7), 559–565.

Zohdi, T. I. and Wriggers, P. (2005). *Introduction to Computational Micromechanics*. Springer.